

RESEARCH ARTICLE

Stat3-Efemp2a modulates the fibrillar matrix for cohesive movement of prechordal plate progenitors

Ting Zhang^{1,*}, Chaoran Yin^{1,*}, Liangjun Qiao^{1,*}, Lulu Jing¹, Hongda Li¹, Chun Xiao¹, Ning Luo¹, Song Lei^{1,2}, Wentong Meng¹, Hongyan Zhu¹, Jin Liu¹, Hong Xu^{1,‡} and Xianming Mo¹

ABSTRACT

Recently, emerging evidence has shown that Stat3 controls tumor cell migration and invasion. However, the molecular mechanisms by which Stat3 controls the cell movement remain largely unknown. Embryonic gastrula progenitors display coordinated and orientated migration, called collective cell migration. Collective cell migration is the simultaneous movement of multiple cells and is universally involved in physiological and pathological programs. Stat3 activity is required for the migration of gastrula progenitors, but it does not affect cell specification, thus suggesting that gastrula movements are an excellent model to provide insight into Stat3 control of cell migration *in vivo*. In this study, we reveal a novel mechanism by which Stat3 modulates extracellular matrix (ECM) assembly to control the coherence of collective migration of prechordal plate progenitors during zebrafish embryonic gastrulation. We show that Stat3 regulates the expression of Efemp2a in the prechordal plate progenitors that migrate anteriorly during gastrulation. Alteration of Stat3-Efemp2a signaling activity disrupted the configuration of fibronectin (FN) and laminin (LM) matrices, resulting in defective coherence of prechordal plate progenitor movements in zebrafish embryos. We demonstrate that Efemp2a acts as a downstream effector of Stat3 to promote ECM configuration for coherent collective cell migrations *in vivo*.

KEY WORDS: Stat3-Efemp2a signaling, Extracellular matrix, Collective cell migration

INTRODUCTION

The Janus kinase-signal transducer and activator of transcription (JAK-STAT) pathway transfers signals derived from intrinsic and environmental stimuli to control the expression of target genes by the binding of STAT proteins to gene promoters (Aaronson and Horvath, 2002). In mammals, there are several STAT genes, including *STAT1*, *STAT2*, *STAT3*, *STAT4*, *STAT5A*, *STAT5B* and *STAT6*. The fact that disruption of the *Stat3* gene leads to early embryonic lethality in mice indicates that Stat3 performs important and unique functions *in vivo* (Takeda et al., 1997). Constitutively active STAT3 has been identified in a number of human tumor types. Emerging evidence shows that STAT3 controls cell migration, motility and invasion in human tumor cells (Azare et al., 2007; Teng et al., 2009). STAT3 has been found to promote tumor invasion and metastasis in various cancers, including ovarian,

bladder, pancreatic and prostate carcinomas and melanoma. Consistent with these pathological roles, conditional knockout of Stat3 in mouse keratinocytes blocks the wound-healing process in skin (Sano et al., 1999). Stat3 has also been found to control the cell migration of mouse embryonic fibroblasts and keloid-derived fibroblasts (Lim et al., 2006). These data suggest that regulation of cell migration is an essential function of Stat3. However, the molecular mechanism by which Stat3 controls cell migration remains largely unknown.

During gastrulation in zebrafish embryonic development, Stat3 is activated on the dorsal side of the embryo via the maternal Wnt/ β -catenin pathway. Stat3 activity is required for the anterior migration of prechordal plate progenitors. Knockdown of Stat3 causes abnormal anterior migration, resulting in a mispositioned head and a shortened anterior-posterior (AP) axis, but produces no defects in early cell fate specification (Yamashita et al., 2002). As a transcription factor, Stat3 controls the expression of downstream genes to regulate essential functions in many biological progresses. For example, Liv1, a breast cancer-associated zinc-transporter protein, functions as a downstream target of Stat3 in the epithelial-mesenchymal transition (EMT) during zebrafish gastrulation (Yamashita et al., 2004). Stat3 has been shown to play crucial roles during gastrulation, and the study of gastrula movements might provide insight into the molecular mechanisms by which Stat3 controls cell migration *in vivo*.

Gastrulation during early embryonic development is an excellent model for the coordinated and orientated cell migration of groups of cells (McMahon et al., 2008; Arboleda-Estudillo et al., 2010; Dumortier et al., 2012). The coordinated and orientated migration of a group of cells, called collective cell migration, is essential for many developmental, physiological and pathological progresses, including embryonic morphogenesis, wound healing, tissue regeneration and invasion of cancers of epithelial origin (Friedl and Gilmour, 2009). A series of collective cell movements, including epiboly, internalization and convergent extension, shapes the basic body plan and forms the embryonic germ layers during embryonic gastrulation (Rohde and Heisenberg, 2007). The key movements of the gastrula cells are convergence and extension movements that narrow and lengthen the embryonic body, respectively. Several distinct cell populations undergo collective cell movements during convergence and extension, including the prechordal plate progenitors migrating toward the animal pole as a cohesive sheet of cells and the lateral mesendoderm cells moving toward the embryonic body axis (Montero et al., 2005; Arboleda-Estudillo et al., 2010).

The EGF-containing fibulin-like extracellular matrix protein 2a (Efemp2, also known as Fibulin 4/Fbln4) is an ECM protein and member of the fibulin family. The fibulin family proteins are characterized by a carboxy-terminal fibulin domain and several repeated calcium-binding epidermal growth factor domains

¹Laboratory of Stem Cell Biology, West China Hospital, Sichuan University, Chengdu 610041, China. ²Department of Pathology, State Key Laboratory of Biotherapy, West China Hospital, Sichuan University, Chengdu 610041, China.

*These authors contributed equally to this work

[‡]Author for correspondence (xuhongm@yahoo.com)

(McLaughlin et al., 2006). Targeted disruption of *Efemp2* abolishes elastogenesis and causes severe lung and vascular defects (McLaughlin et al., 2006). Mutations in *EFEMP2* in humans lead to diaphragmatic hernia, aortic aneurysm, tortuous pulmonary arteries and mild generalized lax skin (Dasouki et al., 2007). During elastogenesis, *Efemp2* tethers lysyl oxidase (LOX) to tropoelastin to form intact elastic fibers (Horiguchi et al., 2009).

In this study, we show that *Stat3* regulates the expression of *efemp2a* in prechordal plate progenitors. In a series of *in vivo* and *in vitro* experiments, we found that *Efemp2a* regulated the cell-driven remodeling of ECM structures and modulated the self-assembly of FN and LM proteins into fibrillar networks. Alteration of *Stat3* or *Efemp2a* activity disorganized the FN and LM fibrillar matrix in zebrafish embryos, resulting in defective coherence in the collective movements of prechordal plate progenitors. *Efemp2a* was able to rescue the defective FN and LM fibrillar matrix and, subsequently, the abnormal coherent migration of gastrula progenitors in *Stat3*-deficient embryos during gastrulation. Our results indicate that *Efemp2a* acts as a downstream effector of *Stat3* to modulate ECM assembly for coherent collective cell migrations *in vivo*.

RESULTS

***Efemp2a* functions as a downstream target of *Stat3* for the gastrula movements during zebrafish embryonic development**

Coherent cell movement is essential for gastrulation. To date, several guidance cues that determine the direction, motility and cohesion of gastrula cell migration have been identified. Among these, *Stat3* activity is required for the anterior migration of prechordal plate progenitors, but it shows no effects on cell fate specification. *Stat3* can serve as an excellent model for understanding the mechanisms by which the gastrula movements are regulated during embryonic development, and we therefore examined the function of *Stat3* in gastrula migration in the zebrafish embryo. First, we screened the gene expression in *Stat3*-deficient embryos. Expression of the gene *efemp2a* was significantly reduced in the prechordal plate progenitors in *Stat3*-depleted conditions at the end of gastrulation, as revealed by *in situ* hybridization (ISH) and whole-mount immunofluorescence staining (Fig. 1A–D,G,H), whereas its expression in other regions, where it might be controlled by other *Stat* proteins (supplementary material Fig. S1), remained normal (Fig. 1E,F). Consistent with these results, the expression of *efemp2a* was elevated or decreased in *stat3*-overexpressing or -depleted embryos as determined by RT-PCR (Fig. 1I). Two-color ISH showed that *efemp2a* was co-expressed with *stat3* in the anterior axial mesendoderm (Fig. 1J). Furthermore, we identified the consensus *Stat3*-binding sites (TTMXXXDAA, D: A, G or T; M: A or C) (Bard et al., 2009) in the *efemp2a* promoter. Chromosome immunoprecipitation (ChIP) analysis showed that FLAG-tagged *Stat3* efficiently immunoprecipitated the proximal promoter regions of *efemp2a* from zebrafish embryo (Fig. 1K), indicating that the *Stat3* protein binds to *efemp2a* promoter sequences *in vivo*. Finally, we injected *efemp2a* mRNA into *Stat3*-depleted embryos, and we observed that the defective anterior migration and convergent movement were rescued (Fig. 1L,M). Together, these data demonstrate that *Efemp2a* functions as a downstream effector of *Stat3* during gastrula movements in zebrafish embryos.

***Stat3*-*Efemp2a* signaling controls coherent migration of prechordal plate progenitors during gastrulation**

To identify the function of *Stat3*-*Efemp2a* signaling for cell migration *in vivo*, we used a translation-blocking antisense

morpholino (tbMO), a splice-blocking morpholino (spMO) and a deletion mutant (C350) to perturb the function of *Efemp2a* (Fig. 4G). C350, the tbMO and the spMO effectively induced similar defects in anterior migration during gastrulation, and the phenotypes were recovered by exogenous *efemp2a* mRNA (supplementary material Fig. S2A). In addition, the tbMO (*Efemp2a*-MO) was able to block both endogenous *Efemp2a* protein expression identified successfully by an antibody against human *Efemp2* protein and exogenous expression of *Efemp2a*-GFP derived from a DNA construct containing the binding site for the tbMO (supplementary material Fig. S2B–D).

We used ISH to examine the expression patterns of several marker genes to investigate in detail the phenotypes caused by *Efemp2*-MO injection. The anterior prechordal plate labeled by *hgg1* (*ctslb* – Zebrafish International Resource Center) was positioned more vegetally and the neural plate marked with *dlx3* (*dlx3b* – Zebrafish International Resource Center) was much broader. The posterior axial mesendoderm and lateral mesoderm, as indicated by *ntl* (*ta* – Zebrafish International Resource Center) and *myod* (*myod1* – Zebrafish International Resource Center), respectively, became wider and shorter at the end of gastrulation in *Efemp2a* morphants (Fig. 2A–D'). The definitive endoderm expressing *sox32* showed no trend toward convergence and the distribution of prechordal plate progenitors expressing *gsc* was disordered in *Efemp2a*-depleted embryos (Fig. 2E–F'). These data indicate that knockdown of *Efemp2a* induces severe impairment in anterior migration and convergent movements, resulting in mispositioning of anterior tissue and a shortened AP axis. However, we observed no significant changes of *ntl*, *lefty* (*lft*) and *gata5* expression, which are related to mesendoderm specification, at the onset of gastrulation in *Efemp2a* morphants (Fig. 2G–J'). Our results indicate that *Efemp2a* function correlates with gastrula migration but not cell specification.

We tracked the prechordal plate progenitors by time-lapse imaging during mid-gastrulation and assessed the cell behaviors as described previously in *Stat3*- or *Efemp2a*-deficient conditions (Kai et al., 2008) (supplementary material Fig. S3A). These monitored cells appeared to move slowly and with reduced coherence and persistence in either *Stat3*-depleted or *Efemp2a*-depleted embryos (Fig. 3A,B). *Efemp2a* mRNA could restore the lower persistence (77.8%, *n*=9) and coherence (66.7%, *n*=9) caused by itself deficiently available, whereas coherence (66.7%, *n*=9) rather than persistence was restored by the addition of *efemp2a* mRNA to *Stat3*-depleted embryos, resulting in recovery of the migration distance along the AP axis (Fig. 3B). Next, we examined the morphology of the prospective prechordal plate undergoing coherent movement. The cells of the leading edge became spherical and separated, and they frequently crawled over one another (supplementary material Fig. S5B,C) in both *Stat3*- and *Efemp2a*-deficient embryos. In particular, there were more spaces between these cells, resulting in a wider region of *gsc* expression in each type of morphant (supplementary material Fig. S5E). In control embryos, the cells were spread and contacted one another (supplementary material Fig. S5A). These morphological changes were consistent with the lower coherence in *Stat3*- or *Efemp2a*-deficient embryos. We also examined the speed, persistence and coherence of lateral mesendoderm cells by differential interference contrast microscope (DIC) time-lapse (supplementary material Fig. S3B and Fig. S4). Neither *Stat3* nor *Efemp2a* induced coherence defects (supplementary material Fig. S4B). These results indicate that *Stat3*-*Efemp2a* signaling mainly controls the coherent migration of

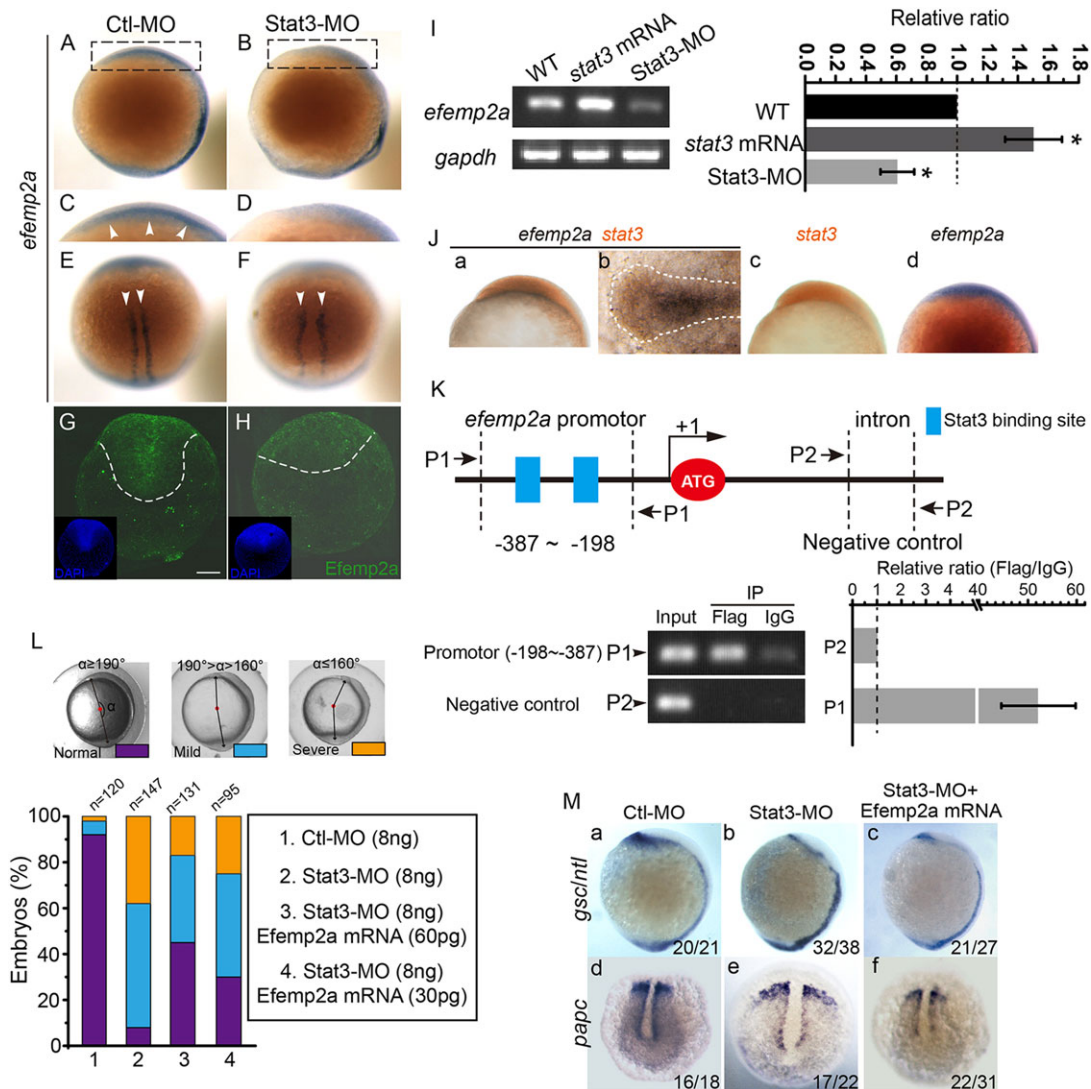


Fig. 1. Efemp2a expression is regulated by Stat3 and rescues the abnormal anterior and convergent migration caused by knockdown of Stat3. (A–F) Stat3 regulates the expression of *efemp2a* in the anterior hypoblast but not in the adaxial region at the end of gastrulation. The arrowheads indicate the region of *efemp2a* expression in the anterior hypoblast (C) and in the adaxial region (E, F). (G, H) Whole-mount immunofluorescence staining for Efemp2a in Ctl-MO- and Efemp2a-MO-injected embryos. The dashed lines indicate the anterior region in G and H. Ctl-MO-injected embryo (A, C, E and G), Stat3-MO-injected embryo (B, D, F and H). Scale bar in G, H: 100 μ m. (I) Overexpression or reduction of Stat3 induced high or low levels of *efemp2a* in zebrafish embryos, respectively. Data were from three independent experiments. * $P < 0.05$ versus control; Student's *t*-test. (J) *efemp2a* and *stat3* colocalized in prechordal plate. Co-staining with *efemp2a* (blue) and *stat3* (orange) by ISH (a, b), *stat3* staining (c), *efemp2a* staining (d). Dashed line in b indicates the prechordal plate. (K) The top panel shows schematic representations of the *efemp2a* promoters. Two pairs of primers were designed to flank the two potential Stat3-binding sites within the *efemp2a* promoter (P1) and a fragment in intron 3 (P2), respectively. The bottom panel shows ChIP analysis of Stat3 in zebrafish embryos. Representative images were from three independent experiments. (L) Exogenous *efemp2a* mRNA rescued the abnormal anterior migration of prechordal plate progenitors in Stat3-MO-injected embryos. α represents the angle from bud to polster. $\alpha \geq 190^\circ$, normal; $190^\circ > \alpha > 160^\circ$, mild phenotype; $\alpha \leq 160^\circ$, severe phenotype. (M) ISH analysis of marker genes during the anterior and convergent migration in embryos. Embryos injected with Ctl-MO (a, d), embryos injected with Stat3-MO (b, e), embryos injected with Stat3-MO + *efemp2a* mRNA (c, f). Lateral views show anterior on the top and dorsal to the right (A–D, Ja, Jc, Jd and Ma–Mc), dorsal views show anterior on the top (E, F), animal-pole views show dorsal on the top (G, H) or on the right (Jb) and ventral-pole views show dorsal on the top (Md–Mf). Embryos were at the tail-bud stage (A–H, J, M).

prechordal plate progenitors and not the persistence, which might be controlled by other Stat3 target genes.

Efemp2a deficiency disrupts focal adhesions, thereby affecting the generation of actin stress fibers and cellular protrusions

As described previously, the oriented protrusions toward the animal pole are required for the anterior migration of prechordal plate progenitors (Dumortier et al., 2012). Three types of cellular protrusions (lamellipodia, filopodia and blebs) have been observed in these progenitors (Diz-Muñoz et al., 2010) (Fig. 4A–C).

We examined the frequency of protrusions from prechordal plate progenitors during mid-gastrulation. When Efemp2a was depleted, the frequency of blebs was significantly increased, accompanied by the generation of fewer filopodia and lamellipodia (Fig. 4D). Lamellipodia and filopodia depend on actin filaments (Diz-Muñoz et al., 2010). Therefore, we injected Lifeact-GFP cDNA into embryos to visualize the changes to actin filaments in actin-rich protrusions. Long protrusions containing actin were detected in control migrating progenitors (Fig. 4Ea–Ee). By contrast, actin formed foci and did not generate lamellipodia or filopodia in Efemp2-deficient progenitors (Fig. 4Ec–Ef).

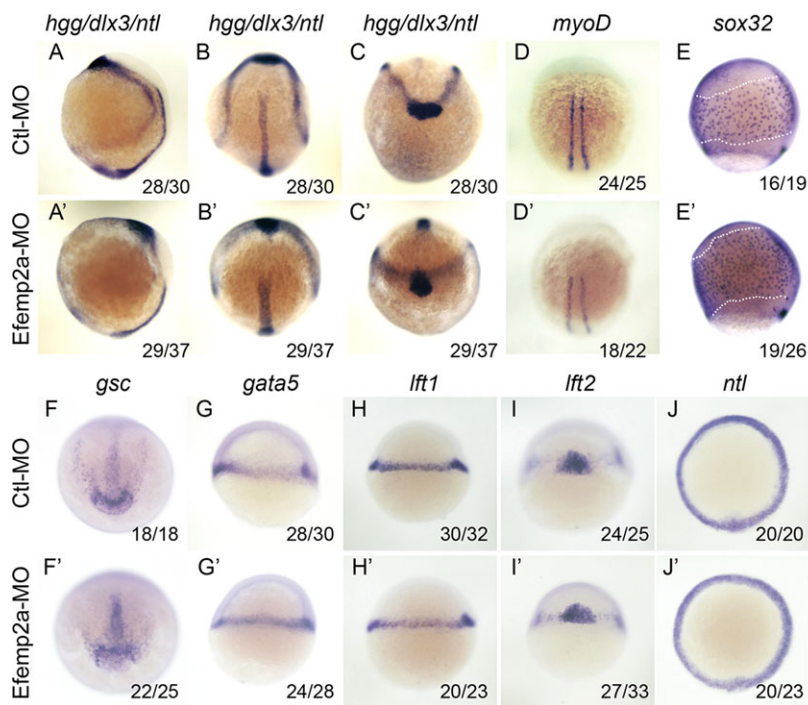


Fig. 2. Knockdown of Efemp2a induces defective anterior migration and convergent movement but does not alter mesendoderm specification during gastrulation.

(A–E') Knockdown of Efemp2a induces defective convergence and extension movement of the mesendoderm during gastrulation in zebrafish embryos. The marker *hgg1* was used to indicate the prechordal plate, *ntl* and *dlx3* marked the prospective notochord and the anterior edge of the neural plate (A–C'), *myoD* indicated the paraxial mesoderm (D,D') and *sox32* labeled the endoderm progenitors (E,E'). The dashed region highlights the distribution of endoderm progenitors (E,E'). (F–J') Inhibition of Efemp2a expression did not influence mesendoderm differentiation. Expression of *gsc* indicated the prechordal plate progenitors (F,F'), *gata5* is a downstream factor of the nodal pathway (G,G'), *lefty* is an antagonist of nodal signaling (H–I') and *ntl* labeled the mesendodermal progenitors (J,J'). Lateral views are shown with anterior on the top and dorsal to the left (A,A',E,E',G,G',H and H'), dorsal views are shown with anterior on the top (B,B',D,D',I and I'), and animal-pole views are shown with dorsal on the top (C,C') or ventral on the top (F,F',J and J'). Embryos were at the tail-bud stage (A–D' and F–F'), 75%-epiboly stage (E–E') or shield stage (G–J').

Previous work has shown that cell migration requires cellular protrusions to couple to the ECM through the plasma membrane via focal adhesions (Gupton and Waterman-Storer, 2006). Focal adhesions that are formed by adhesion complexes perform crucial scaffolding and signaling roles in the interaction of cells with the ECM (Carragher and Frame, 2004). Therefore, we detected the focal adhesion components Fak (Protein tyrosine kinase 2ab/Ptk2ab – Zebrafish International Resource Center) and Vinculin in the prechordal plate region. Focal adhesions were dramatically diminished or disrupted in Efemp2a-deficient embryos (Fig. 4F). This phenotype was also observed in cultured HUVEC cells infected with an adenovirus expressing Efemp2a full-length protein or its mutant C350 on FN or LM substrate. Both Efemp2a and C350 were able to disrupt the formation of focal adhesions and actin fibers in cells (Fig. 4H,I). Together, these results suggest that the decrease in focal adhesions disrupts the formation of actin-based cellular protrusions in Efemp2a-deficient embryos, and there is probably a correlation between the reduction in focal adhesions and the ECM.

Efemp2a interacts with soluble FN and LM to shape their matrices

To understand the character of Efemp2a, we transplanted prechordal mesendodermal (PCME) cells from the shield of Efemp2a-MO-injected or Ctl-MO-injected donors into the shield of wild-type or Efemp2a-depleted host embryos and monitored their migration (supplementary material Fig. S6A,C). We also co-transplanted lateral mesendodermal (LME) cells from Efemp2a-MO or Ctl-MO donors into the lateral blastoderm margin of wild-type or Efemp2a-depleted host embryos (supplementary material Fig. S6B,D). These results demonstrate that Efemp2a plays a non-cell-autonomous role in controlling the migration of gastrula cells. Combined with immunoblots of human cells ectopically expressing Efemp2a, these results confirm that Efemp2a is an extracellular protein (supplementary material Fig. S6E).

Efemp2a has been reported previously to promote the assembly of Elastin, an ECM component, and we therefore examined the expression of elastin during gastrulation. FN and LM, two other

ECM components (supplementary material Fig. S7B,C), but not Elastin (supplementary material Fig. S7A), were expressed during gastrulation in zebrafish embryos. Therefore, we hypothesized that Efemp2a acts on the expression or function of FN or LM. The mRNA expression levels of FN and LM were not altered in Efemp2a-depleted embryos (supplementary material Fig. S8). Subsequently, we examined the interaction between Efemp2a and FN or LM via co-immunoprecipitation. The collected culture media containing abundant GFP-tagged Efemp2a or C350, and little FN and LM (Fig. 5B,G,M–O), were incubated with or without soluble FN or LM. After overnight incubation, the supernatant and deposition were separated from each mixture by centrifugation. The supernatants were subjected to immunoprecipitation with anti-GFP, anti-FN or anti-LM antibody, and the GFP-tagged proteins were observed to actively associate with FN or LM (Fig. 5D–F,I–L). By contrast, few GFP fusion proteins were detected in depositions containing abundant FN or LM (Fig. 5P–T), and it was likely that a fraction of Efemp2a, C350 and GFP non-specifically followed insoluble polymers during centrifugation (Fig. 5U). These immunoprecipitation assays indicate that Efemp2a and its mutant C350 are able to interact with soluble FN and LM. However, these interactions cannot maintain binding with insoluble polymers of FN and LM, suggesting that Efemp2a is involved in the function of FN and LM.

Next, we examined FN and LM self-assembly with and without Efemp2a or the C350 mutant *in vitro*. FN and LM proteins were able to self-assemble into fine fibers with branches in the presence of fetal bovine serum (FBS) or only bovine serum albumin (BSA) in Hanks' Balanced Salt Solution (HBSS) (Fig. 6Ba,Be). In the presence of purified GFP-tagged Efemp2a, the FN and LM fibers became more branched and thicker, respectively (Fig. 6Aa,Bb,Bd,Bf,Bh), and then the depositions of FN and LM became larger and denser than the controls (Fig. 6Ca,Cb,Cd,Ce,Cg,Ch). In the presence of the C350-GFP, both LM and FN assembled short fibers with fewer branches, which were hardly able to form fine depositions (Fig. 6Bc,Bd,Bg,Bh, Cc,Cf–Ch). Altogether, Efemp2a displays a modulatory function on the assembly of FN and LM into insoluble fibrillar meshwork. Given

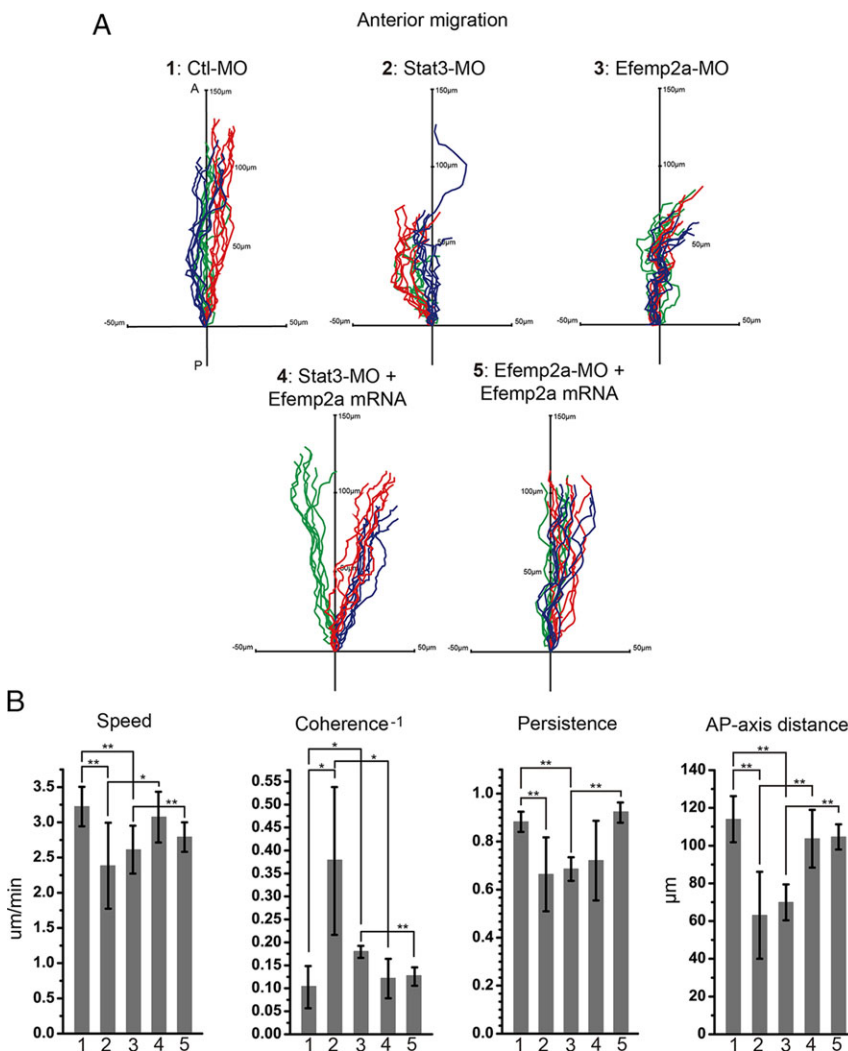


Fig. 3. Stat3-Efemp2a signaling controls the coherent migration of prechordal plate progenitors. (A) Tracks of the monitored prechordal plate progenitors in the embryo injected with Ctl-MO, Stat3-MO, Efemp2a-MO, Stat3-MO combined with *efemp2a* mRNA or Efemp2a-MO combined with *efemp2a* mRNA. Three clusters, including six neighboring cells, are highlighted in different colors. (B) Analyzed parameters: speed, coherence, persistence and distance. * $P < 0.05$, ** $P < 0.01$ versus control; Student's *t*-test.

the multi-cellular microenvironment *in vivo*, we tested the effect of Efemp2a on ECM formation in cultured MDCK or HeLa cells. These cells, which were infected with or without C350 adenovirus (Ad-C350), were cultured with different concentrations of recombinant EFEMP2 in combination with FN or LM. Excess EFEMP2 protein could promote FN and LM deposition compared with control, and the stimulatory effects depended on the dose of EFEMP2 (supplementary material Fig. S9Aa–Ad, Ba–Bd). By contrast, in cells overexpressing the C350 mutant, the assembly of FN and LM was perturbed, resulting in failure to generate fine FN or LM matrices (supplementary material Fig. S9Af, Bf). Notably, the effect of EFEMP2 could be disrupted by the Efemp2a mutant C350 protein (supplementary material Fig. S9Ae, Be). Thus, Efemp2a can, indeed, further FN and LM assembly.

Stat3-Efemp2a controls the configuration of the ECM for the gastrula migration in zebrafish embryos

We next assessed whether knockdown of Efemp2a or Stat3 disrupted ECM assembly *in vivo*. Immunostaining in whole embryos and 10-µm sections of zebrafish embryos was performed to examine the structure of the ECM. In the control embryos and sections, FN and LM ECM assembled continuous fibrillar matrices in the anterior regions (Fig. 7Aa, Af, Ba, Bg). By contrast, the fibrillar meshworks of FN and LM were disrupted in Efemp2a- or Stat3-deficient embryos, and the deposition of FN

and LM was scattered (Fig. 7Ab, Ac, Ag, Ah, Bb, Bc, Bh, Bi). The ECM defects in Efemp2a- or Stat3-depleted embryos were rescued by an appropriate level of supplementation with zebrafish *efemp2a* mRNA (Fig. 7Ad, Ae, Ai, Aj, Bd, Be, Bj, Bk). However, overexpression of *efemp2a* mRNA also disrupted the continuous FN and LM ECM fibrillar matrix and induced the formation of dense foci within the gastrulae (Fig. 7Bf, Bl). Examination of the embryo ultrastructure also showed defective ECM in the Stat3- or Efemp2a-deficient embryos (Fig. 7C). It has been reported that the assembly and three-dimensional fibrillar organization of FN regulate cell adhesion, spreading and migration in *Xenopus* embryos (Darribère and Schwarzbauer, 2000; Rozario et al., 2009). The 70-kD N-terminal fragment of FN (70 kD-FN) was shown to obstruct FN matrix formation (Rozario et al., 2009). We confirmed that 70 kD-FN perturbed the formation of the FN fibrils *in vitro* and in zebrafish embryos (supplementary material Fig. S10A–F). Tracking the migrating prechordal plate progenitors in the embryos injected with 70 kD-FN revealed that the assembly of FN fibrils was blocked by 70 kD-FN, resulting in low persistence and coherence during cell migration (supplementary material Fig. S10G, H). In addition, when the FN matrix assembly was disrupted, the leading edge cells in the prechordal plate also became spherical and separated, with more interspace (supplementary material Fig. S5D). The loose cell contact resulted in extended field of *gsc* expression

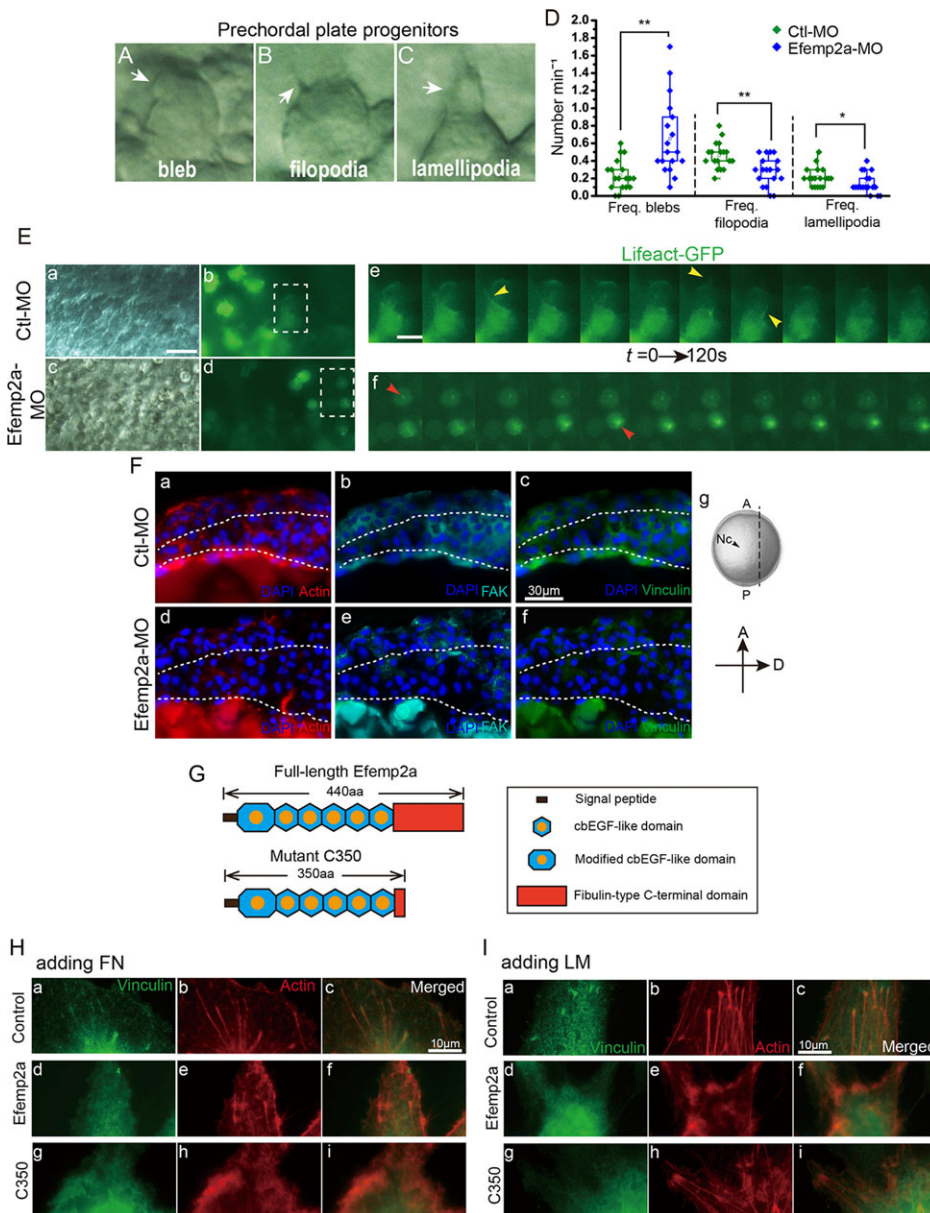


Fig. 4. Efemp2a controls cellular protrusions by influencing focal adhesion. (A–C) Bleb, filopodia and lamellipodia were detected during the anterior movements of prechordal plate progenitors. The arrows indicate blebs (A), filopodia (B) and lamellipodia (C). (D) Frequency of bleb, filopodium and lamellipodium formation in control and Efemp2a-deficient leading edge cells of prechordal plate. * $P < 0.05$, ** $P < 0.01$ versus control; Student's t -test. (E) Lifeact-GFP cDNA was injected into embryos at the one-cell stage and images were obtained during mid-gastrulation: DIC images (a,c), fluorescence (b,d) and magnified views (e,f) of the regions marked by dashed boxes in b and d. Cells were injected with Lifeact-GFP and actin dynamics were visualized during prechordal plate progenitor migration (e,f). Yellow arrowheads indicate the actin-rich cell protrusions in normal cells; red arrowheads indicate abnormal actin aggregation in Efemp2a-deficient cells. Scale bars: 20 μ m in a; 10 μ m in e. (F) Analysis of the focal adhesion complex marked by Fak and Vinculin staining in sagittally sectioned bud-stage embryos pre-injected with Ctl-MO (a–c) or Efemp2a-MO (d–f). Scheme shows sagittal section. A, anterior; P, posterior; D, dorsal; Nc, notochord (g). Dashed lines indicate the prechordal plate. Lateral views are shown with anterior on the top and dorsal to the left. Scale bar: 30 μ m (g) Schematic of the Efemp2a protein and its mutant C350. (H,I) HUVECs were cultured on cover glasses with FN or LM and infected by adenoviruses to overexpress GFP, Efemp2a-GFP and C350-GFP. These cells were then fixed and co-stained for F-actin and Vinculin to show the actin stress fibers and focal adhesion complexes. Scale bars: 10 μ m. Embryos were at the 75%-epiboly stage (A–E) or tail-bud stage (F).

(supplementary material Fig. S5E). These phenotypes are highly similar to those caused by the disruption of Stat3-Efemp2a signaling. Collectively, these results indicate that Stat3-Efemp2a signaling modulates ECM assembly for the cohesive migration of prechordal plate progenitors in embryos during gastrulation.

Previous studies have shown that disruption of the ECM or Stat3 can cause an epithelial-mesenchymal transition (EMT) (Yamashita et al., 2004; Radisky, 2005). However, ISH showed that the expression of EMT marker genes, including *e-cadherin* (*cdh1* – Zebrafish International Resource Center), *tp1a*, *n-cadherin* (*cdh2* – Zebrafish International Resource Center) and *snail1b*, were not coincident changes following alteration of *efemp2a* activity *in vivo* (supplementary material Fig. S11A). *In vitro*, the protein expression level of EMT markers, including E-cadherin, ZO-1, N-cadherin and Zeb1, were also not significantly changed in cultured HeLa cells overexpressing Efemp2a or C350 (supplementary material Fig. S11B). These results exclude the possibility that a shift of the activity in Efemp2a induces EMT to affect the migration of gastrula cells.

Moreover, we detected the expression of focal adhesion receptors, including *itgav*, *itgb1* and *sdca4*, in Efemp2a-depleted embryos. These results showed that *itgav* expression was reduced, but *itgb1* and *sdca4* expression levels were increased in the prechordal plate region (supplementary material Fig. S12). Thus, the data do not indicate that Efemp2a controls ECM assembly through the integrin or syndecan pathways.

In summary, we show that Stat3 controls *efemp2a* expression in the prechordal plate progenitor cells (supplementary material Fig. S13). Efemp2a protein is secreted to promote FN and LM assembly into a matrix. The proper FN and LM fibrillar matrices maintain collective migration for correct embryonic development at early stages. Because ECM assembly and collective cell migration are involved in cell proliferation, differentiation, migration and survival in many biological processes, such as immune response, hematopoiesis, neurogenesis and tumorigenesis, our study provides new insights into the molecular mechanisms underlying how ECM assembly and collective cell migration may function together to perform these biological processes *in vivo*.

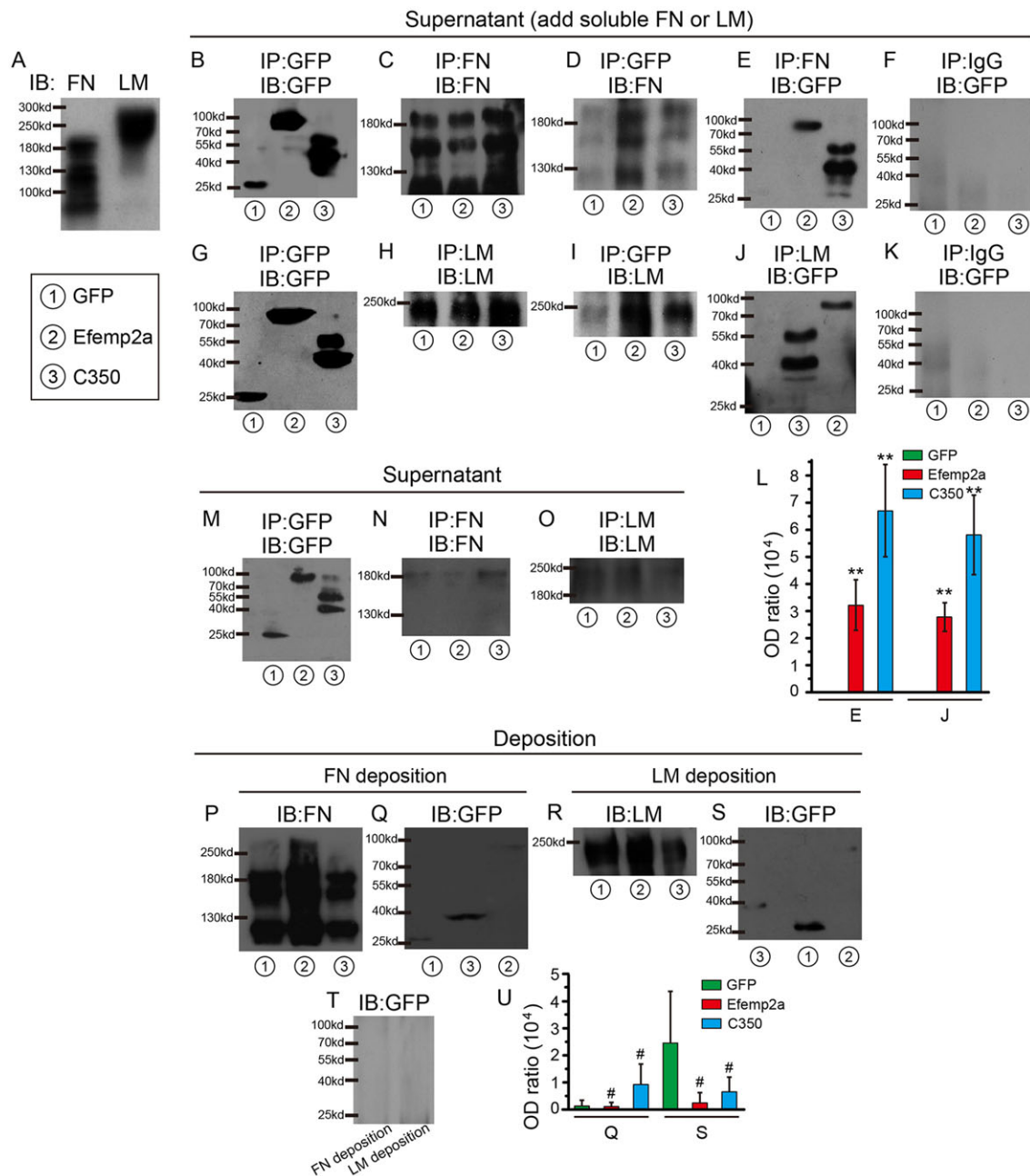


Fig. 5. The interaction between Efemp2a and soluble FN or LM. (A) The specific bands of the FN and LM on the gel. (B-U) Efemp2a and its mutant C350 could interact with FN and LM in the supernatant (D,E,I,J) but not in the deposition (Q,S). AD293 cells were infected with adenoviruses expressing GFP, Efemp2a-GFP or C350-GFP, respectively, and the media were collected after 48 h and co-incubated with (B-K) or without soluble FN or LM (M-O). Then, the supernatant (B-O) and deposition (P-U) were separated by centrifugation. The supernatant underwent co-immunoprecipitation with anti-GFP (B,D,G,I,M), FN (C,E,N) or LM (H,J,O) antibodies or IgG (F,K). F and K show the negative controls for E and J. (L) The OD ratios of GFP, Efemp2a or C350 bands (E,J) to negative controls (F,K). FN or LM deposition was formed in DMEM without GFP, Efemp2a or C350 in T. T is the negative control for Q and S. (U) The OD ratios of GFP, Efemp2a or C350 bands (Q,S) to negative controls (T). The OD value was defined as 1 when no specific bands were observed in gels. Data were derived from three independent experiments (L,U). # $P > 0.05$, ** $P < 0.01$ versus GFP group; Student's *t*-test.

DISCUSSION

Efemp2a controls the proper spatiotemporal formation of FN and LM fibrillar matrix *in vivo*

In the present study, we found that Efemp2a was expressed earlier than tropoelastin during embryonic development, indicating that Efemp2a performs unknown functions during early embryonic development. Indeed, the results presented here demonstrate that Efemp2a performs an essential function in the modulation of FN and LM assembly *in vitro* or *in vivo*. We show that FN and LM undergo self-assembly

in vitro. Under conditions of HBSS with serum or BSA, FN and LM are able to form fine fibrils with branches. Full-length Efemp2a increases the branching of FN and the average diameter of LM fibers. These FN or LM fibrils form larger and denser depositions compared with controls. The Efemp2a mutant, C350, reduces the ability of both FN and LM to form fine fibrils with branches, and these short fibrils do not readily generate a fine meshwork. *In vivo*, knockdown of *efemp2a* expression in zebrafish embryos disrupts the assembly of FN and LM into fibrillar meshwork. In addition, overexpression of

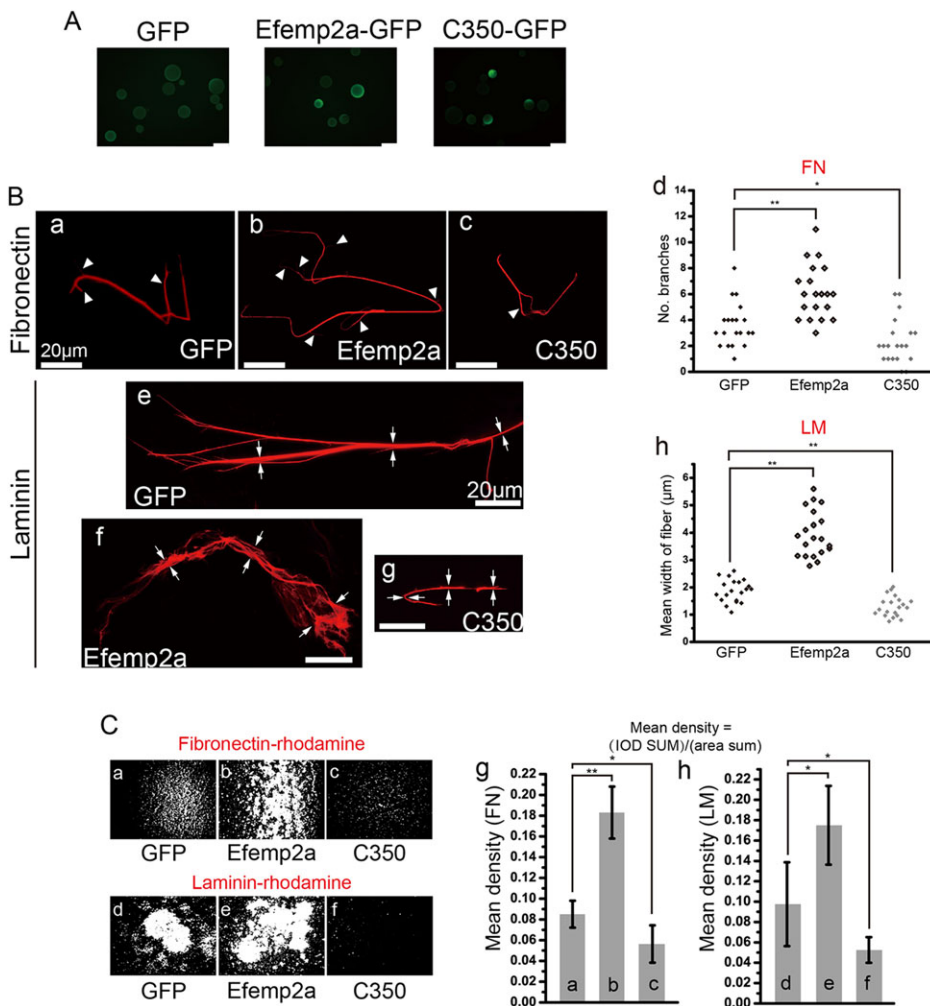


Fig. 6. Efemp2a modulates the self-assembly of FN and LM *in vitro*. (A) Agarose beads absorb fluorescent proteins via immunoprecipitation. Adenoviruses overexpressing GFP, Efemp2-GFP or C350-GFP were used to infect AD293 cells and the cell lysates were collected. Samples were incubated with Protein A/G beads and anti-GFP antibody. Scale bars: 200 μm. (B) Efemp2a activity modulates the self-assembly of FN and LM into fibers *in vitro*. Soluble FN (a-c) or LM (e-g) spontaneously assembled into fibers in the presence of GFP (a,e), Efemp2a (b,f) or C350 (c,g) beads. The arrowheads indicate the branches in a-c; the widths of the regions labeled by arrows are measured in e-g. Quantification of the branch numbers of FN fibers (d) or the mean widths of LM fibers (h). Scale bars: 20 μm. (C) Efemp2a activity affects the polymerization and deposition of FN and LM. FN-Rhodamine (a-c) or LM-Rhodamine (d-f) deposition by self-assembly. Quantification of the mean density of FN-Rhodamine or LM-Rhodamine deposition (g,h). * $P < 0.05$, ** $P < 0.01$ versus control; Student's *t*-test.

efemp2a mRNA induces the formation of FN and LM foci. These results are consistent with previous observations that FN and LM assembled into fibers and fibrillar matrices without any additional enzymatic proteins and/or energy (Ulmer et al., 2008). Here, we show that Efemp2a can interact with soluble FN and LM. Increased or decreased *efemp2a* expression, or overexpression of its mutant, is able to disrupt the fine FN and LM fibrillar matrix, but it does not disturb the assembly of FN and LM *in vitro* and *in vivo*. These findings indicate that the function of Efemp2a in the formation of FN and LM fibrillar matrix is different from its role in the formation of elastic fibers. These data also indicate that Efemp2a directly promotes the assembly of LM and FN to form a matrix without the assistance of other enzymatic proteins. Additional *in vitro* biochemical experiments are required to address the biochemical mechanism by which Efemp2a molds the LM and FN matrix.

Stat3-Efemp2a shapes the matrix path for coherent collective migration

We analyzed the behavior of gastrula progenitors via time-lapse movies of living zebrafish embryos during gastrulation and observed that the prechordal plate progenitors migrate directionally as a group with cell-cell connections, consistent with previous findings (Dumortier et al., 2012; Tada and Heisenberg, 2012). During migration, the leader cells of the group extend forward by cell protrusions. As described previously, we also noticed that, during the progression of migration, the gastrula progenitors continuously

express E-Cadherin along the interface between the epiblast and hypoblast throughout gastrulation (Montero et al., 2005).

On close review of the video data, we noticed that the collective migration of the prechordal plate progenitors is highly similar to the multicellular broad and flat rim of epithelial sheet migration (Khalil and Friedl, 2010). The leading edge cells in the migrating sheet of gastrula progenitors explore the environment, identify the migration path and form traction. As described previously, during the process of collective migration, the migrating cells make physical contact with the adjacent matrix (Montell, 2008). The contacts and subsequent crosstalk between the cells and matrix lead to the generation of a fibrillar matrix that acts as a track and supports the migration processes (Winklbauer and Nagel, 1991; Wang et al., 2008). The matrix track has structural and molecular properties that can perform additional functions in addition to guiding the direction of cell migration. For example, the newly formed matrix promotes the maintenance of collective front-rear polarity during collective cell migration. Indeed, we find that proper FN and LM assembly into a matrix beneath deep mesendoderm cells coincides with the migration of prechordal plate progenitors, suggesting that the FN and LM fibrillar matrix supports and directs the collective cell migration of gastrula progenitors. Under conditions in which knockdown of Efemp2a expression disrupts the structures of FN and LM matrix, the gastrula progenitors maintain their mobility and randomize migrating direction as individual cells, rather than as a coherent group of cells. The randomized migration of the

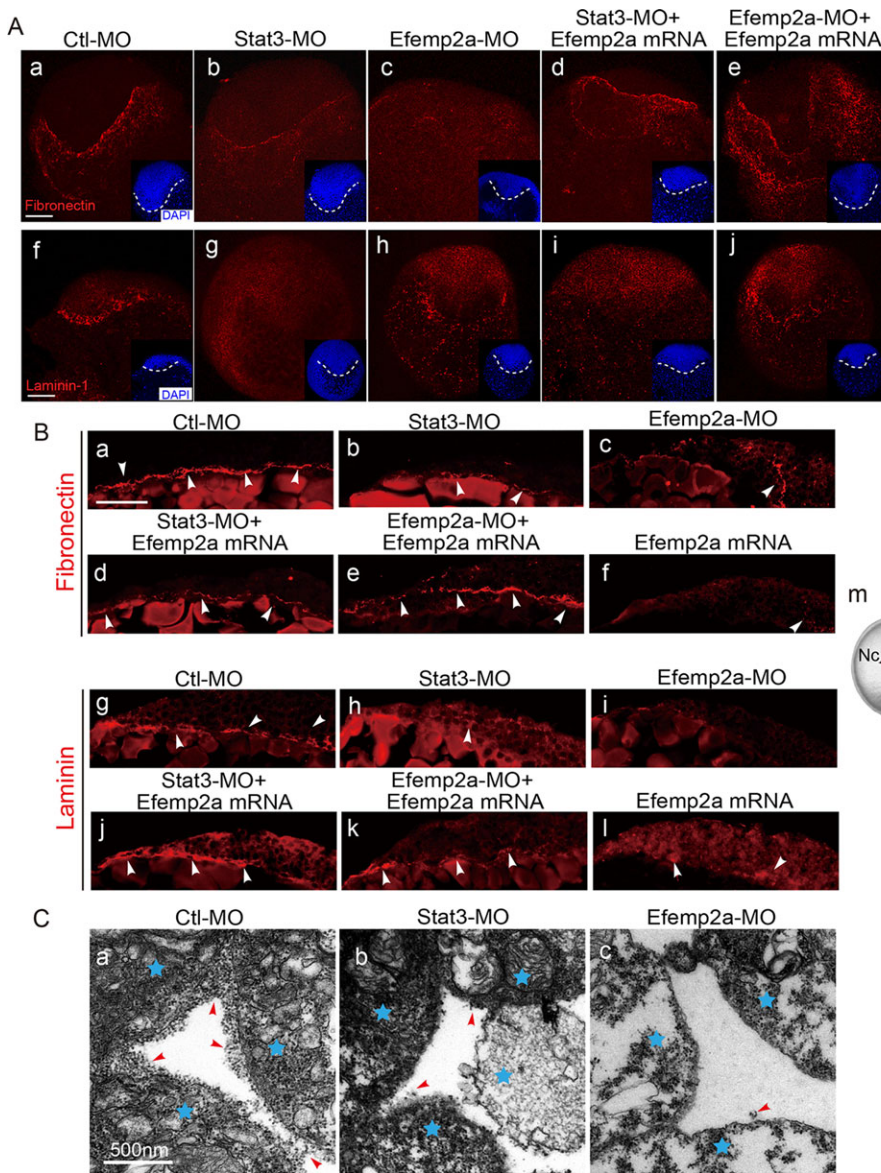


Fig. 7. Efemp2a activity modulates the assembly of FN and LM in zebrafish embryos. (A) Whole-mount immunofluorescence staining for FN (a–e) and LM (f–j) in embryos injected with Ctl-MO (a,f), Stat3-MO (b,g), Efemp2a-MO (c,h), Stat3-MO combined with *efemp2a* mRNA (d,i) or Efemp2a-MO combined with *efemp2a* mRNA (e,j). Dashed lines indicate the leading edge of the prechordal plate in DAPI staining images. Animal-pole views show dorsal on the top. Scale bars: 100 μ m. (B) Immunostaining analysis of the FN and LM matrix in sagittally sectioned embryos, injected with Ctl-MO (a,g), Stat3-MO (b,h), Efemp2a-MO (c,i), Stat3-MO combined with *efemp2a* mRNA (d,j), Efemp2a-MO combined with *efemp2a* mRNA (e,k) or *efemp2a* mRNA (f,l) at the end of gastrulation, using FN (a–f) and LM (g–l) antibodies. The arrowheads indicate the FN or LM matrix. Scheme shows sagittal section. A, anterior; P, posterior; Nc, notochord (m). Lateral views show dorsal to the right and anterior on the top. Scale bar: 200 μ m. (C) TEM of sagittally sectioned embryos injected with Ctl-MO (a), Stat3-MO (b) or Efemp2a-MO (c) at the end of gastrulation. The arrowheads indicate the ECM structure and asterisks highlight the cells. Embryos were at the tail-bud stage (A–C). Scale bar: 500 nm.

progenitors causes a mispositioned head and a shortened AP axis during gastrulation. These results indicate that the proper FN and LM fibrillar meshwork beneath deep mesendodermal cells is required for maintaining collective migration and for ensuring the appropriate direction of migration of the prechordal plate progenitors for correct embryonic development.

During embryonic gastrulation, the ECM components LM and FN are highly expressed in the anterior regions and form a continuous fibrillar meshwork. The ECM assembly is controlled by Stat3-Efemp2a signaling. Ectopic expression of *efemp2a* can rescue the ECM defects and the lower coherence of migrating prechordal plate progenitors caused by Stat3 deficiency. In conclusion, our data demonstrate that Efemp2a is an effector of Stat3 signaling and plays a non-cell-autonomous role to control the coherence of cellular migration in gastrulation in zebrafish embryos.

MATERIALS AND METHODS

Zebrafish strains

Zebrafish were raised and maintained following standard procedure. Wild-type zebrafish belonged to the AB strain. All experiments involving the use of animals were conducted in compliance with the approved guidelines. The

animal protocols were approved by the Animal Care and Use Committee of West China Hospital, Sichuan University, China.

Efemp2a cloning

Efemp2a cDNA was amplified from zebrafish embryos using the primers 5'-ATCCAATGCGGGCCTGTTCTC-3' and 5'-ACAATCTCGGAAAT-GCCGTCTG-3' and subcloned into the pGEM-T easy vector to synthesize antisense or sense probes for *in situ* hybridization. The coding region of Efemp2a was subcloned into the pcDNA3.1 vector for mRNA synthesis.

In situ hybridization

The *efemp2a* antisense RNA probe was synthesized using a digoxigenin RNA labeling kit (Roche). Whole-mount *in situ* hybridization was performed as previously described (Thisse and Thisse, 2008).

Morpholino knockdown

Efemp2a tbMO (5'-CCGCATCCTCACACCCCCTTCAAC-3'), the primary MO used, targets the 5' sequence spanning the start codon, and Efemp2a spMO (5'-AGGTTTCGTTCTCCTTACCGTGA-3') blocks the splicing of *efemp2a* mRNA. Stat3 MO (5'-GCCATGTTGACCCCT-TAATGTGTCG-3') and Stat5.1 MO (5'-CTTGTGACTTACCAGAGT-TGTCC-3') were reported in previous studies (Yamashita et al., 2002; Liu et al., 2009). A standard control MO was used as the control.

Construction of Efemp2a mutants

Six mutants of zebrafish Efemp2a were designed based on conserved domain analysis and generated by PCR. The C-terminal deletion mutants included C70, C140, C210, C280 and C350. The N-terminal deletion N10 mutant lacks the signal peptide. Capped *efemp2a* mutant mRNA and full-length mRNA that lacked the morpholino sequence were synthesized as previously described (Zhang et al., 2011).

Microinjection

Injection of mRNA constructs or morpholinos was performed at the one- to four-cell stages. In all experiments, 8 ng Efemp2a-tbMO, Efemp2a-spMO or Stat3-MO was injected with 80 pg C350 mRNA. For the overexpression experiment, 100 pg *efemp2a* mRNA was also injected. For recovery experiments, 60 pg or 30 pg *efemp2a* mRNA was also injected.

Immunofluorescence staining

Immunofluorescence staining was performed as previously described (Zhang et al., 2011) using the following antibodies: anti-Efemp (Abnova, H00030008-M01; 1:400); anti-Fibronectin (Sigma, F3684; 1:400); anti-Laminin-1 (Thermo Scientific, RB-082-A1; 1:400); anti-Fak (Santa Cruz, sc-558; 1:500); and anti-Vinculin (Millipore, MAB3574; 1:500).

Time-lapse imaging and cell movement analysis

Time-lapse imaging of zebrafish embryos during gastrulation was performed as previously described (Arboleda-Estudillo et al., 2010). Embryos were flat-mounted and imaged under a Leica DM6000B fluorescence microscope or SP5 confocal microscope with 20× or 40× objectives. Images were taken at one frame per 30 s for 80 cycles during tracking of prechordal plate progenitors or at one frame per 20 s for 60 cycles during monitoring of lateral mesendoderm. ImageJ (NIH) software was used to track randomly chosen cells in every frame and to calculate parameters including speed, persistence and coherence as previously described (Kai et al., 2008; Arboleda-Estudillo et al., 2010). For analysis of the frequency of cellular protrusions, frames were captured at 12 s intervals for 10 min by DIC time-lapse using a Zeiss Imager Z1 microscope with a 20× objective. Three independent experiments were performed, and Student's *t*-test was used to evaluate comparisons between two groups.

Cell transplantation

Embryos were injected with Ctl-MO combined with FITC-dextran (Invitrogen) or with Efemp2a-MO combined with Rhodamine-dextran (Invitrogen), and donor cells were harvested. Cells were transplanted into wild-type host embryos or Efemp2a-MO-injected host embryos as previously described (Yao et al., 2010).

FN and LM self-assembly *in vitro*

Media were collected from cultured AD293 cells overexpressing GFP, Efemp2a-GFP or C350-GFP from adenovirus infection. The 10 ml of harvested culture medium was mixed with 20 µl Protein A/G agarose beads and 2 µg anti-GFP antibody (Novus, NBP1-47584; 1:5000). The mixtures were rotated overnight at 4°C and then centrifuged at 1000 rpm for 1 min. The harvested beads absorbed GFP, Efemp2a-GFP or C350-GFP protein. These agarose beads were combined with 4 µg soluble FN or LM and added into 1 ml HBSS with 10% FBS or 1% BSA, and these mixtures were rotated for 1 h at room temperature (RT). Next, the mixtures were centrifuged at 3000 rpm for 5 min, and immunofluorescence staining was performed for the precipitations, which included the insoluble production by FN or LM self-assembly and agarose beads, using anti-FN (Sigma, F3684; 1:500) or anti-LM (Thermo Scientific, RB-082-A1; 1:500) antibody. Finally, the precipitations were dropped onto glass slides, mounted and then observed using a fluorescence microscope. For measurements of mean density of the FN or LM matrix, Rhodamine-tagged FN or LM (Cytoskeleton) was used. The agarose beads absorbing GFP, Efemp2a-GFP or C350-GFP, together with 4 µg Rhodamine-tagged FN or LM, were added into 1 ml HBSS with 1% BSA and incubated for 1 h at RT. The mixtures were dropped onto glass slides, mounted and observed using a fluorescence microscope. The mean density (IOD sum/area sum) was measured by Image-Pro Plus 6.0 software.

Immunoprecipitation and immunoblotting

The media from cultured AD293 cells overexpressing GFP, Efemp2a-GFP or C350-GFP by adenovirus infection were collected. Soluble FN (Millipore) or LM (Sigma) was added into the medium and incubated for 1 h at RT. The supernatant and deposition were separated by centrifugation at 3000 rpm for 5 min. The supernatant, protein A/G agarose beads (Millipore) and antibody (anti-GFP, anti-FN or anti-LM antibody) were mixed and rotated overnight at 4°C. The agarose beads were harvested by centrifugation at 1000 rpm for 1 min and then washed three times. Samples were separated by SDS-PAGE, followed by electrophoretic transfer onto a membrane. The membranes were blocked and immunoblotting was performed using the following antibodies: anti-Fibronectin (Sigma, F3684; 1:1000), anti-Laminin-1 (Thermo Scientific, RB-082-A1; 1:1000) and anti-GFP (Novus, NBP1-47584; 1:1000). The GFP-tagged FN and LM in depositions were also detected by western blotting.

Chromosome immunoprecipitation assay

ChIP was performed as described previously (Liu et al., 2012). Briefly, 150 embryos were injected with Stat3-Flag plasmid and harvested at the 20-somite stage. The embryos were placed in 1% formaldehyde, homogenized and then sonicated to generate 300–500 bp chromatin fragments. Fragmented chromatin was immunoprecipitated with Flag (Sigma, F1804; 1:1000) or IgG (Santa Cruz, sc-2025; 1:250) antibody. Nucleic acids were precipitated with 100% ethanol and used for PCR. Primer P1: 5'-CAATGCGAGTACAAATATTGCA-3' and 5'-TTAATCACACGGTTCCTAAATA-3'; primer P2: 5'-ACAACA-GGACACCGCAGATTT-3' and 5'-TTTATGCCCATTTCCACCGT-3'.

Cell culture

The cell lines AD-293, MDCK and HUVEC were cultured in Dulbecco's modified Eagle's medium (DMEM) containing 10% fetal calf serum (FCS). HeLa cells were cultured in RPMI-1640 medium containing 10% FCS. All cultures were incubated at 37°C with 5% CO₂. Medium was changed every 48 h. Soluble FN or LM and recombinant Efemp2 protein (Abnova) were added to the medium when required for the experiment.

Construction and infection of adenovirus

The recombinant adenovirus plasmids obtained by AdEasy technology were digested with *PacI* and transfected into AD-293 cells using transfection reagents as described previously (Luo et al., 2007). After collection of the supernatants from primary viral transfection, AD-293 cells were infected by viral supernatants for the amplification and purification of high-titer recombinant adenoviruses. The cultured HeLa cells, HUVEC cells or MDCK cells were infected by viral supernatants containing high-titer recombinant adenoviruses. After 24 h, the infected cells were harvested for use in immunofluorescent staining.

Acknowledgements

The authors thank the members of the Mo laboratory for their critical discussion and review of the manuscript. The authors thank Christopher Brooks, Ph.D., of Bioscience Editing Solutions, for language assistance.

Competing interests

The authors declare no competing financial interests.

Author contributions

T.Z. and C.Y. designed, performed and analyzed experiments, and wrote this manuscript. L.Q. helped with the molecular and biochemical experiments. L.J., H.L., C.X. and N.L. helped with the molecular experiments; and S.L. helped with the transmission electron microscope experiment. W.M., H.Z. and J.L. helped with experimental analysis; and X.M. helped with experimental analysis and writing. H.X. conceived this study, designed the experiments, analyzed the data and wrote this manuscript.

Funding

This work was supported by the National Basic Research Program of China [2009CB941200 to X.M.], the Nature Science Foundation of China [31171384 to H.X.], and the Key Project of Chinese Ministry of Education [109136 to X.M.].

Supplementary material

Supplementary material available online at <http://dev.biologists.org/lookup/suppl/doi:10.1242/dev.104885/-/DC1>

References

- Aaronson, D. S. and Horvath, C. M. (2002). A road map for those who don't know JAK-STAT. *Science* **296**, 1653-1655.
- Arboleda-Estudillo, Y., Krieg, M., Stühmer, J., Licata, N. A., Muller, D. J. and Heisenberg, C. P. (2010). Movement directionality in collective migration of germ layer progenitors. *Curr. Biol.* **20**, 161-169.
- Azare, J., Leslie, K., Al-Ahmadie, H., Gerald, W., Weinreb, P. H., Violette, S. M. and Bromberg, J. (2007). Constitutively activated Stat3 induces tumorigenesis and enhances cell motility of prostate epithelial cells through integrin beta 6. *Mol. Cell. Biol.* **27**, 4444-4453.
- Bard, J. D., Gelebart, P., Amin, H. M., Young, L. C., Ma, Y. and Lai, R. (2009). Signal transducer and activator of transcription 3 is a transcriptional factor regulating the gene expression of SALL4. *FASEB J.* **23**, 1405-1414.
- Carragher, N. O. and Frame, M. C. (2004). Focal adhesion and actin dynamics: a place where kinases and proteases meet to promote invasion. *Trends Cell Biol.* **14**, 241-249.
- Darribère, T. and Schwarzbauer, J. E. (2000). Fibronectin matrix composition and organization can regulate cell migration during amphibian development. *Mech. Dev.* **92**, 239-250.
- Dasouki, M., Markova, D., Garola, R., Sasaki, T., Charbonneau, N. L., Sakai, L. Y. and Chu, M.-L. (2007). Compound heterozygous mutations in fibulin-4 causing neonatal lethal pulmonary artery occlusion, aortic aneurysm, arachnodactyly, and mild cutis laxa. *Am. J. Med. Genet. A* **143A**, 2635-2641.
- Diz-Muñoz, A., Krieg, M., Bergert, M., Ibarlucea-Benitez, I., Muller, D. J., Paluch, E. and Heisenberg, C.-P. (2010). Control of directed cell migration in vivo by membrane-to-cortex attachment. *PLoS Biol.* **8**, e1000544.
- Dumortier, J. G., Martin, S., Meyer, D., Rosa, F. M. and David, N. B. (2012). Collective mesendoderm migration relies on an intrinsic directionality signal transmitted through cell contacts. *Proc. Natl. Acad. Sci. USA* **109**, 16945-16950.
- Friedl, P. and Gilmour, D. (2009). Collective cell migration in morphogenesis, regeneration and cancer. *Nat. Rev. Mol. Cell Biol.* **10**, 445-457.
- Gupton, S. L. and Waterman-Storer, C. M. (2006). Spatiotemporal feedback between actomyosin and focal-adhesion systems optimizes rapid cell migration. *Cell* **125**, 1361-1374.
- Horiguchi, M., Inoue, T., Ohbayashi, T., Hirai, M., Noda, K., Marmorstein, L. Y., Yabe, D., Takagi, K., Akama, T. O., Kita, T. et al. (2009). Fibulin-4 conducts proper elastogenesis via interaction with cross-linking enzyme lysyl oxidase. *Proc. Natl. Acad. Sci. USA* **106**, 19029-19034.
- Kai, M., Heisenberg, C.-P. and Tada, M. (2008). Sphingosine-1-phosphate receptors regulate individual cell behaviours underlying the directed migration of prechordal plate progenitor cells during zebrafish gastrulation. *Development* **135**, 3043-3051.
- Khalil, A. A. and Friedl, P. (2010). Determinants of leader cells in collective cell migration. *Integr. Biol.* **2**, 568-574.
- Lim, C. P., Phan, T.-T., Lim, I. J. and Cao, X. (2006). Stat3 contributes to keloid pathogenesis via promoting collagen production, cell proliferation and migration. *Oncogene* **25**, 5416-5425.
- Liu, Y.-H., Jakobsen, J. S., Valentin, G., Amarantos, I., Gilmour, D. T. and Furlong, E. E. M. (2009). A systematic analysis of Tinman function reveals Eya and JAK-STAT signaling as essential regulators of muscle development. *Dev. Cell* **16**, 280-291.
- Liu, F., Yao, S., Zhang, T., Xiao, C., Shang, Y., Liu, J. and Mo, X. (2012). Kzr regulates the transcription of gata2 and pu.1 during primitive hematopoiesis in zebrafish embryos. *J. Genet. Genomics* **39**, 463-471.
- Luo, J., Deng, Z.-L., Luo, X., Tang, N., Song, W.-X., Chen, J., Sharff, K. A., Luu, H. H., Haydon, R. C., Kinzler, K. W. et al. (2007). A protocol for rapid generation of recombinant adenoviruses using the AdEasy system. *Nat. Protoc.* **2**, 1236-1247.
- McLaughlin, P. J., Chen, Q., Horiguchi, M., Starcher, B. C., Stanton, J. B., Broekelmann, T. J., Marmorstein, A. D., McKay, B., Mecham, R., Nakamura, T. et al. (2006). Targeted disruption of fibulin-4 abolishes elastogenesis and causes perinatal lethality in mice. *Mol. Cell. Biol.* **26**, 1700-1709.
- McMahon, A., Supatto, W., Fraser, S. E. and Stathopoulos, A. (2008). Dynamic analyses of Drosophila gastrulation provide insights into collective cell migration. *Science* **322**, 1546-1550.
- Montell, D. J. (2008). Morphogenetic cell movements: diversity from modular mechanical properties. *Science* **322**, 1502-1505.
- Montero, J.-A., Carvalho, L., Wilsch-Bräuninger, M., Kilian, B., Mustafa, C. and Heisenberg, C.-P. (2005). Shield formation at the onset of zebrafish gastrulation. *Development* **132**, 1187-1198.
- Radisky, D. C. (2005). Epithelial-mesenchymal transition. *J. Cell Sci.* **118**(Pt 19), 4325-4326.
- Rohde, L. A. and Heisenberg, C.-P. (2007). Zebrafish gastrulation: cell movements, signals, and mechanisms. *Int. Rev. Cytol.* **261**, 159-192.
- Rozario, T., Dzamba, B., Weber, G. F., Davidson, L. A. and DeSimone, D. W. (2009). The physical state of fibronectin matrix differentially regulates morphogenetic movements in vivo. *Dev. Biol.* **327**, 386-398.
- Sano, S., Itami, S., Takeda, K., Tarutani, M., Yamaguchi, Y., Miura, H., Yoshikawa, K., Akira, S. and Takeda, J. (1999). Keratinocyte-specific ablation of Stat3 exhibits impaired skin remodeling, but does not affect skin morphogenesis. *EMBO J.* **18**, 4657-4668.
- Tada, M. and Heisenberg, C.-P. (2012). Convergent extension: using collective cell migration and cell intercalation to shape embryos. *Development* **139**, 3897-3904.
- Takeda, K., Noguchi, K., Shi, W., Tanaka, T., Matsumoto, M., Yoshida, N., Kishimoto, T. and Akira, S. (1997). Targeted disruption of the mouse Stat3 gene leads to early embryonic lethality. *Proc. Natl. Acad. Sci. USA* **94**, 3801-3804.
- Teng, T. S., Lin, B., Manser, E., Ng, D. C. H. and Cao, X. (2009). Stat3 promotes directional cell migration by regulating Rac1 activity via its activator betaPIX. *J. Cell Sci.* **122**(Pt 22), 4150-4159.
- Thisse, C. and Thisse, B. (2008). High-resolution in situ hybridization to whole-mount zebrafish embryos. *Nat. Protoc.* **3**, 59-69.
- Ulmer, J., Geiger, B. and Spatz, J. P. (2008). Force-induced fibronectin fibrillogenesis in vitro. *Soft Matter* **4**, 1998-2007.
- Wang, X., Ohlin, C. A., Lu, Q. and Hu, J. (2008). Cell directional migration and oriented division on three-dimensional laser-induced periodic surface structures on polystyrene. *Biomaterials* **29**, 2049-2059.
- Winklbauer, R. and Nagel, M. (1991). Directional mesoderm cell migration in the Xenopus gastrula. *Dev. Biol.* **148**, 573-589.
- Yamashita, S., Miyagi, C., Carmany-Rampey, A., Shimizu, T., Fujii, R., Schier, A. F. and Hirano, T. (2002). Stat3 controls cell movements during zebrafish gastrulation. *Dev. Cell* **2**, 363-375.
- Yamashita, S., Miyagi, C., Fukada, T., Kagara, N., Che, Y.-S. and Hirano, T. (2004). Zinc transporter LIV1 controls epithelial-mesenchymal transition in zebrafish gastrula organizer. *Nature* **429**, 298-302.
- Yao, S., Qian, M., Deng, S., Xie, L., Yang, H., Xiao, C., Zhang, T., Xu, H., Zhao, X., Wei, Y.-q. et al. (2010). Kzr controls canonical Wnt8 signaling to modulate dorsoventral patterning during zebrafish gastrulation. *J. Biol. Chem.* **285**, 42086-42096.
- Zhang, T., Yao, S., Wang, P., Yin, C., Xiao, C., Qian, M., Liu, D., Zheng, L., Meng, W., Zhu, H. et al. (2011). ApoA-II directs morphogenetic movements of zebrafish embryo by preventing chromosome fusion during nuclear division in yolk syncytial layer. *J. Biol. Chem.* **286**, 9514-9525.

Supplementary Information

Figure S1. The expression of *efemp2a* in paraxial mesoderm is regulated by Stat5.1.

(A) The expression pattern of *efemp2a* in paraxial mesoderm. (B) The expression pattern of *stat5.1* in paraxial mesoderm. (C, D) Knockdown *stat5.1* induced reduction of *efemp2a* expression. Ctl-MO injected embryo (C), Stat5.1-MO injected embryo (D). Embryos were the tail-bud stage and dorsal views are shown with anterior on the top (A-D).

Figure S2. Disruption of Efemp2a function blocks the anterior migration of prechordal plate progenitors during gastrulation.

(A) Quantification of the phenotypes induced by micro-injection experiments. (B) Anti-human Efemp2 antibody was able to detect the zebrafish Efemp2a-GFP fused protein. (C) Endogenous Efemp2a expression was identified through immunoblot using Anti-human Efemp2 antibody in Ctl-MO and Efemp2a-MO -injected embryos at bud stage. (D) Efemp2a-MO inhibited the expression of the zebrafish Efemp2a-GFP fusion protein in zebrafish embryos at the 75%-epiboly stage.

Figure S3. Monitoring the tracks of the signed cell clusters during anterior migration or convergent movement.

(A, B) Three clusters including six cells were randomly highlighted in different colors among the prechordal plate progenitors (A) or lateral mesendodermal cells (B) in control, Stat3-depleted, Efemp2a-deficient or recovered embryos. Cell tracks are displayed in figure 2A and S4A. Animal-pole views are shown with dorsal on the top (A), lateral views are shown with anterior on the top and dorsal to the right (B). Embryos were the 75%-epiboly stage (A, B).

Figure S4. Stat3-Efemp2a signaling does not control the coherence of lateral mesendodermal cells during convergent migration.

(A) Tracks of the monitored lateral mesendodermal cells in the embryo injected with Ctl-MO, Stat3-MO, Efemp2a-MO, Stat3-MO combined with Efemp2a mRNA or Efemp2a-MO

combined with Efemp2a mRNA. Three clusters including six neighboring cells highlighted in different colors. (B) Analyzed parameters: speed, coherence, persistence and distance. * $P < 0.05$, ** $P < 0.01$ versus control, ns: no significant, t-test.

Figure S5. Defective ECM induces abnormal morphology of prechordal plate progenitors during gastrulation.

(A-D) The morphology of prechordal plate progenitors in Ctl-MO (A), Efemp2a-MO (B), Stat3-MO (C) or 70 kD-FN (D) -injected embryos. The magnified views of the regions marked by dashed rectangles in A-D (a-d). (E) *gsc* marked the region of prechordal plate in Ctl-MO (a), Stat3-MO (b), Efemp2a-MO (c) or 70 kD-FN (d) -injected embryos. w: the width of *gsc* expression. Dash line indicated the width of *gsc* expression. Quantification of the width of *gsc* expression (e). Embryos were the 75%-epiboly stage (A-E). ** $P < 0.01$ versus control, t-test.

Figure S6. Efemp2a is an extracellular protein and plays a non-cell autonomous role.

(A, C) Prechordal mesendodermal (PCME) cells from wild-type (green) or Efemp2a-deficient donors (red) were transplanted into the inner domain of the shield of a wild-type or Efemp2a-deficient host. Images were taken at the end of gastrulation. (B, D) Lateral mesendodermal (LME) cells from wild-type (green) or Efemp2a-deficient (red) donors were transplanted into the lateral side of a wild-type or Efemp2a-deficient host. Images were taken at the end of gastrulation. Lateral views are shown with anterior on the top and dorsal on the right (A, C); dorsal views are shown anterior on the top (B, D). (E) Adenoviruses overexpressing GFP or Efemp2-GFP were used to infect AD293 cells, and the culture medium was collected. Through immunoprecipitation, GFP-tagged Efemp2a rather than β -actin was detected in the culture medium. Embryos were the tail-bud stage (A-D).

Figure S7. FN and LM rather than Elastin are expressed at gastrulation in zebrafish embryo.

(A) The expression of elastin was detected by RT-PCR at early gastrulation and 10 dpf. (B, C) *fn1* and *lamb1* expression were examined by ISH at bud stage. Dashed indicated the region of

prechordal plate. Embryos were the tail-bud stage and animal views are shown with ventral on the top (B, C).

Figure S8. Alteration of Efemp2a activity does not affect the expression of FN and LM.

RT-PCR was used to detect expression of fibronectin and three subunits of laminin-1 at shield, 75%-epiboly and bud stages. Expression of *gapdh* was used as RNA loading control.

Figure S9. The recombinant Efemp2 promotes the assembly of FN and LM mediated by cultured cell *in vitro*.

(A) MDCK cells were cultured on coverglass slips. Adding recombinant Efemp2 (1ug) and FN (10ug) (a, e), recombinant Efemp2 (0.5ug) and FN (10ug) (b), recombinant Efemp2 (0.1ug) and FN (10ug) (c) or FN (10ug) (d, f) into culture medium. Cells were infected by adenovirus expressing C350 (AD-C350) in e, f. g is blank control. (B) HeLa cells were cultured on coverglass slips. Adding recombinant Efemp2 (1ug) and FN (10ug) (a, e), recombinant Efemp2 (0.5ug) and FN (10ug) (b), recombinant Efemp2 (0.1ug) and FN (10ug) (c) or FN (10ug) (d, f) into culture medium. Cells were infected by adenovirus expressing C350 (AD-C350) in e, f. g is blank control.

Figure S10. FN matrix influences gastrula movements.

(A-D) 70 kD-FN interfered the assembly of WT FN *in vitro*. Adding FN (10ug) (A), FN (10ug) combined with 70 kD-FN (5ug) (B), 70 kD-FN (5ug) (C) into the medium of cultured MDCK cells. D is blank control. (E, F) Whole-mount immunohistochemistry staining for BSA (0.8ug/ul) or 70 kD-FN (0.8ug/ul) -injected embryos. Dashed indicated the region of prechordal plate. (G) Tracks of the monitored prechordal plate progenitors in the embryo injected with BSA or 70 kD-FN. Three clusters including six neighboring cells highlighted in different colors. (B) Analyzed parameters: speed, persistence and coherence. Embryos were the tail-bud stage (E, F). * $P < 0.05$, ** $P < 0.01$ versus control, t-test.

Figure S11. Alteration of Efemp2a activity does not induce EMT.

(A) The expression of EMT marker genes, including *e-cadherin* (a-c), *tjp1a* (d-e), *n-cadherin* (g-i) and *snailb* (j-l) were detected by ISH in zebrafish embryos injected with Ctl-MO, Efemp2a or Efemp2a mRNA. (B) HeLa cells overexpressing GFP, Efemp2a or C350 by

adenovirus infection were assessed for expression levels of the EMT marker proteins by immunoblot. E-cadherin, Zo1 were epithelial markers; N-cadherin and Zeb1 were used as mesenchymal markers. Embryos were the tail-bud stage (A). Animal-pole views are shown with ventral on the top (Aa-Ac, Aj-Al), lateral views are shown with anterior on the top and dorsal to the right (Ad-Ai).

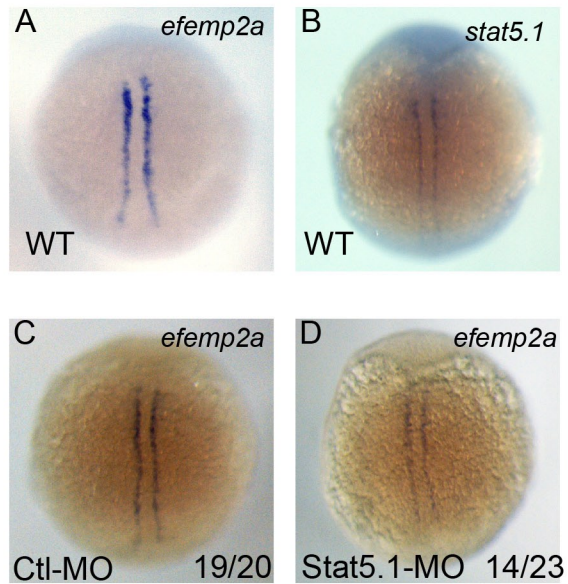
Figure S12. The changes of the focal adhesion receptors expression in Efemp2a-deficient embryos.

(A-F) Detection of the expression of *itgaV* (A, B), *itgb1* (C, D) and *sdca4* (E, F) via ISH at bud stage. Animal-pole views are shown with ventral on the top (A-D), lateral views are shown with anterior on the top and dorsal to the right (E, F).

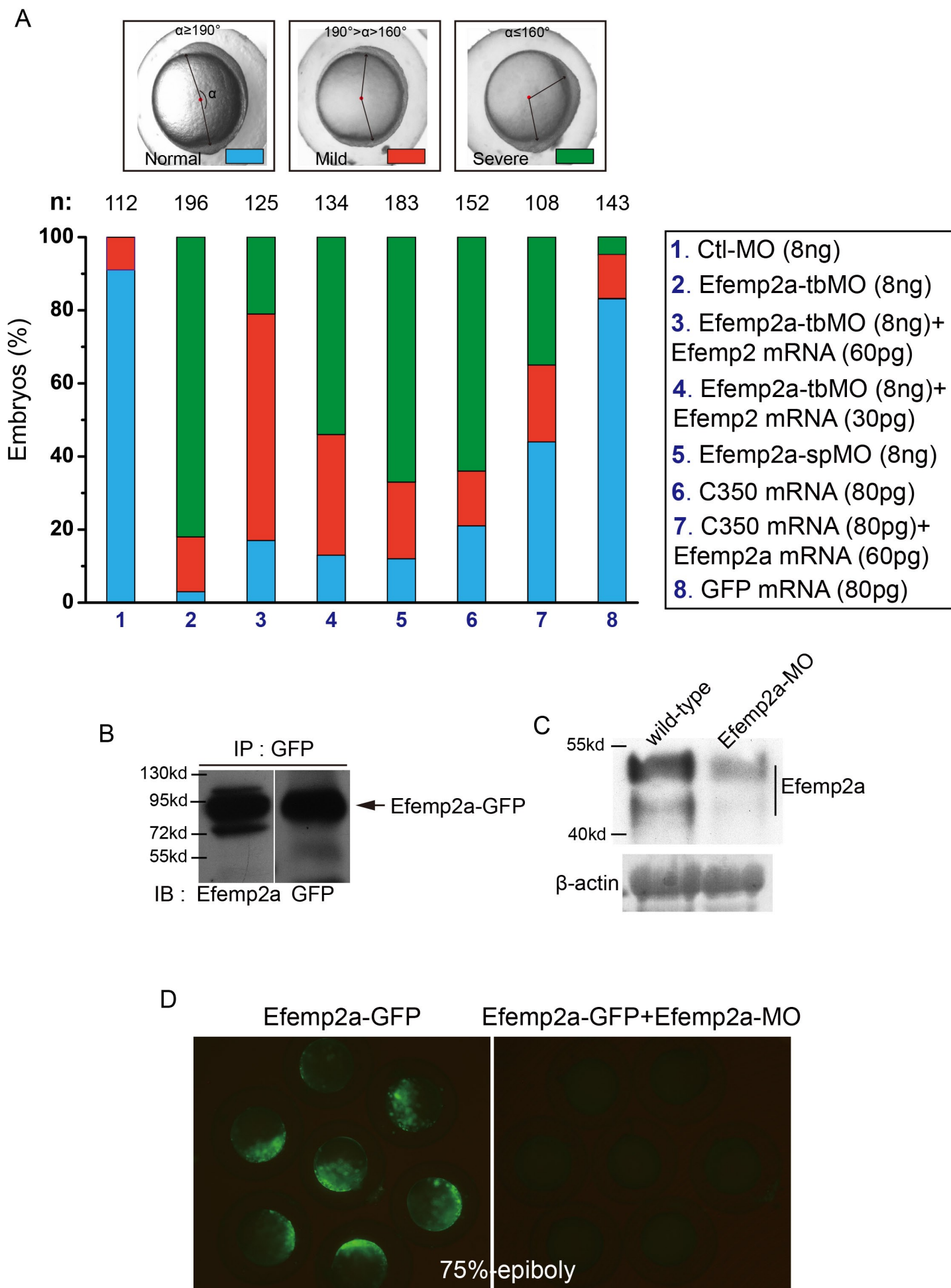
Figure S13. A proposed model for the role of Stat3-Efemp2a signaling during the embryonic cells collective migration.

Stat3 regulates the expression of Efemp2a playing non cell-autonomous role. Efemp2a promotes FN and LM assembly into correct matrix to control coherence of multi-cell migration. The other Stat3 downstream targets, X proteins function as cell-autonomous role and mainly regulate the cellular persistence and mobility during cell movements.

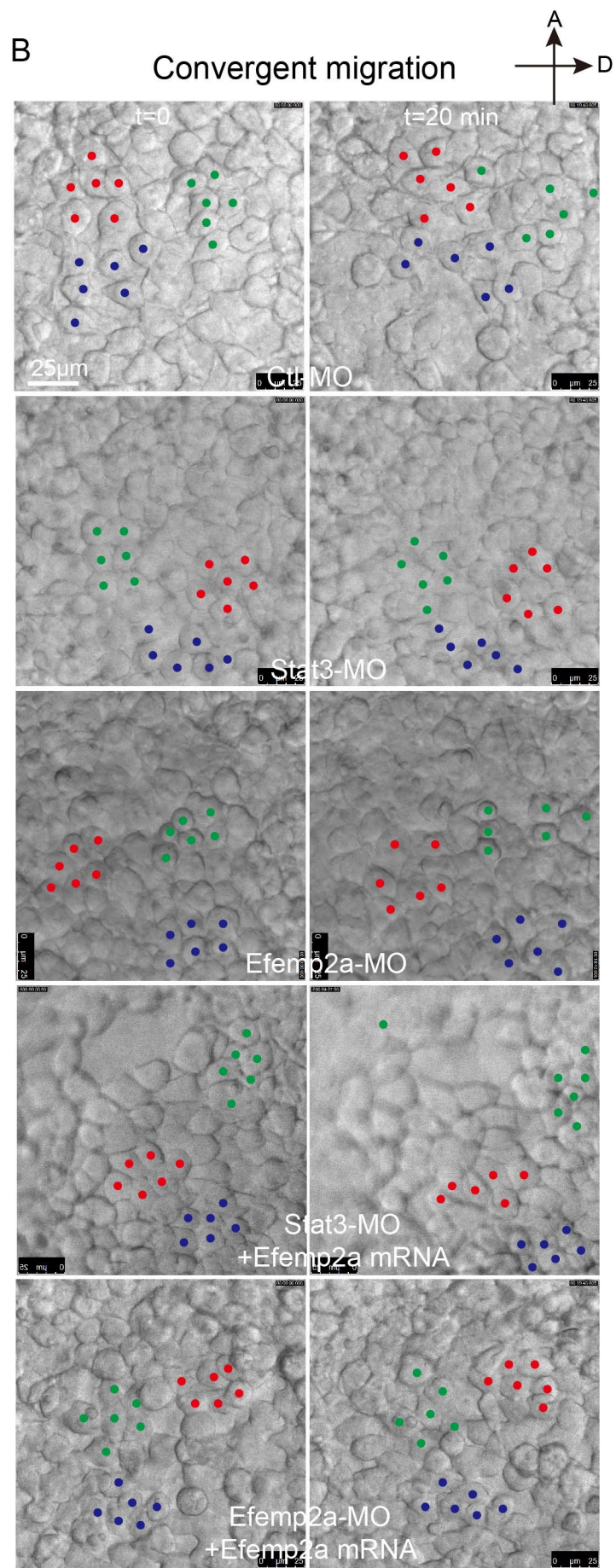
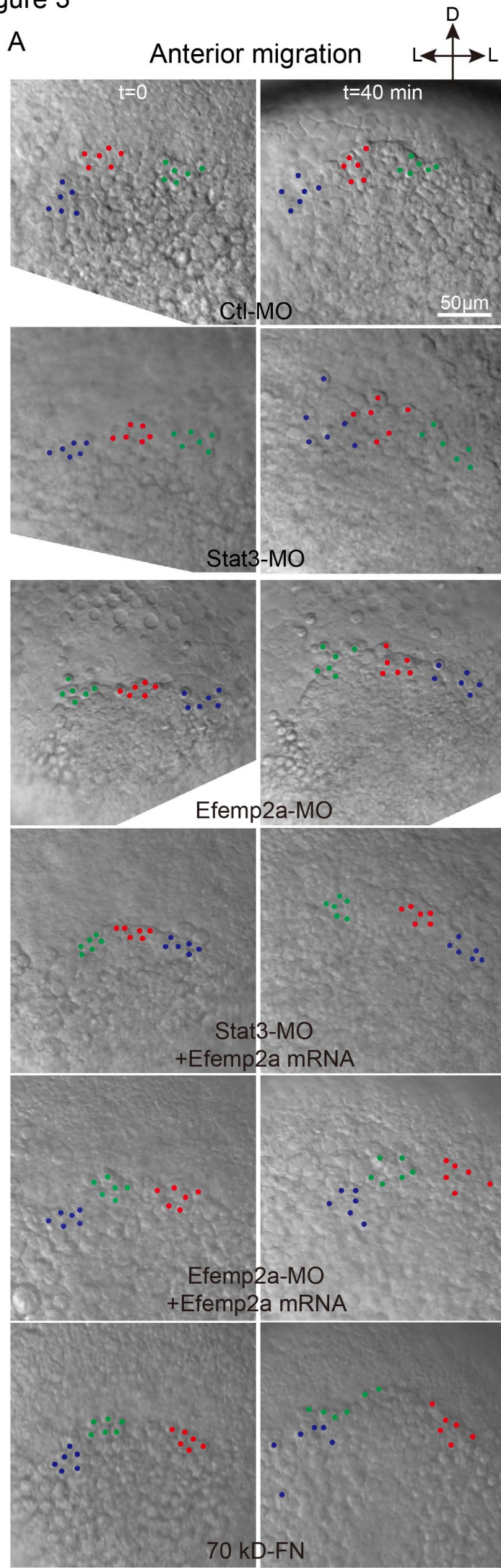
Sfigure 1



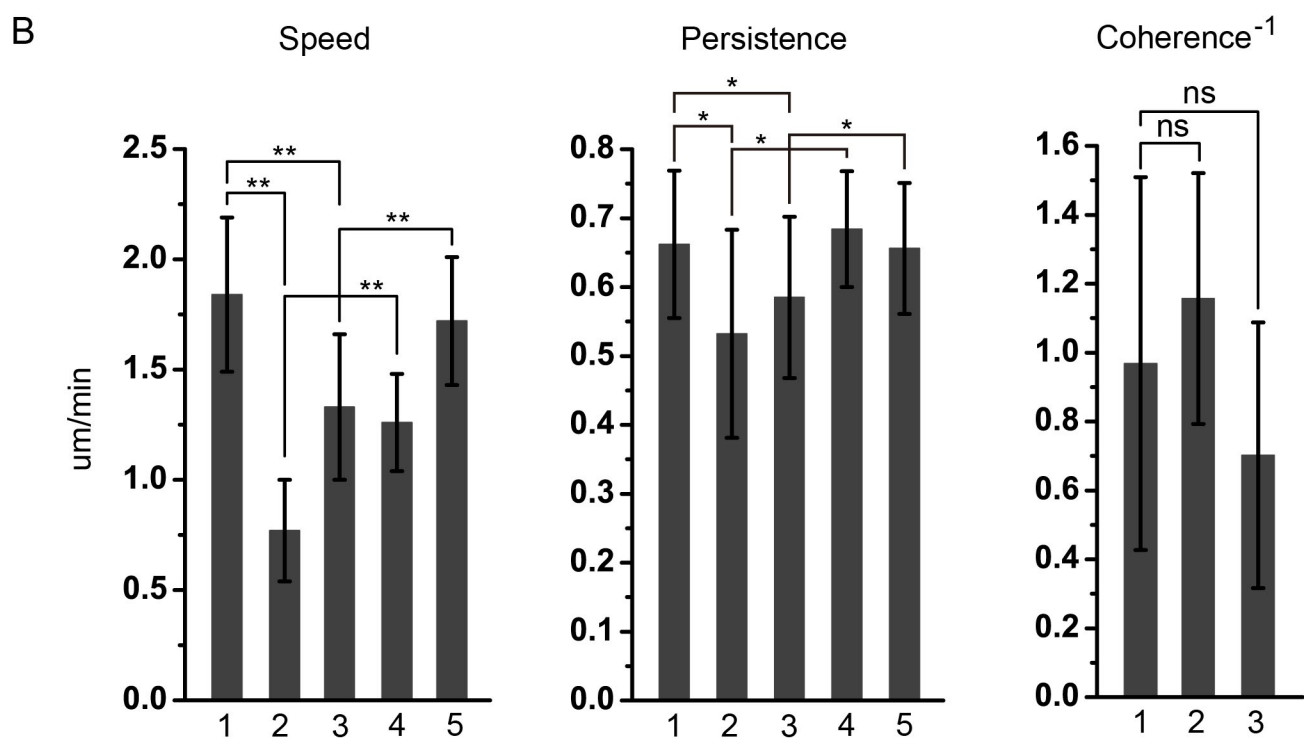
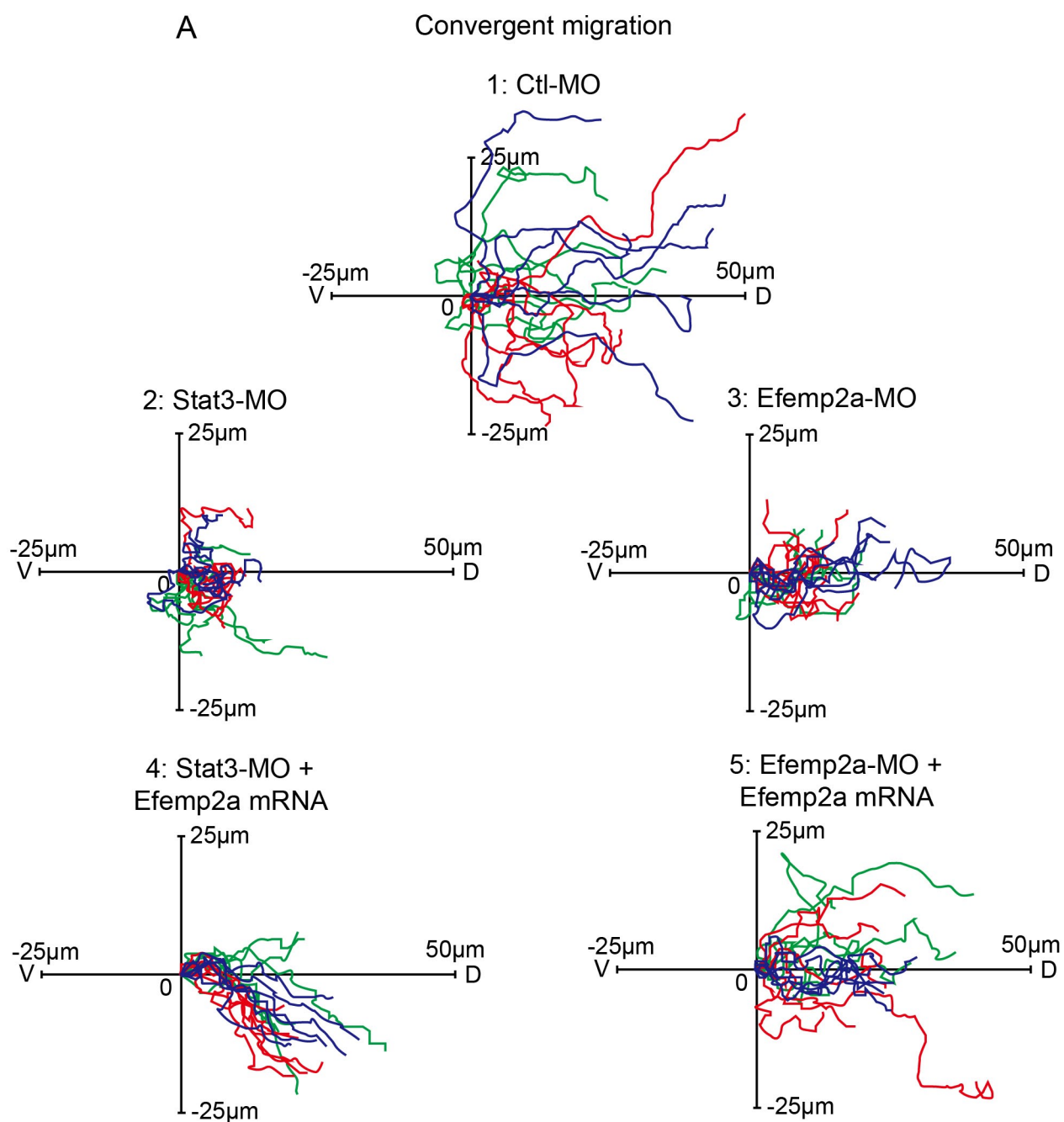
Sfigure 2



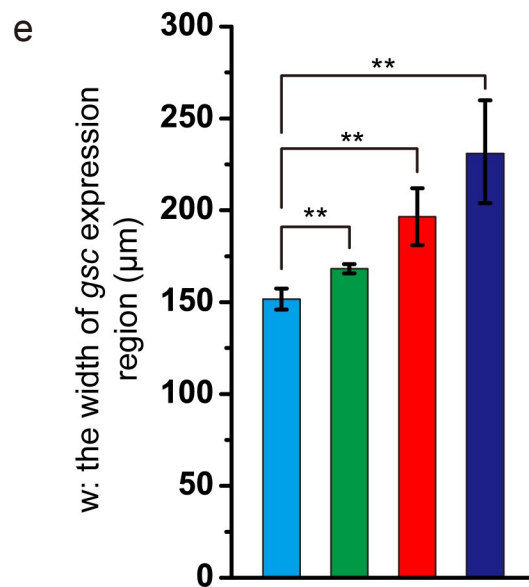
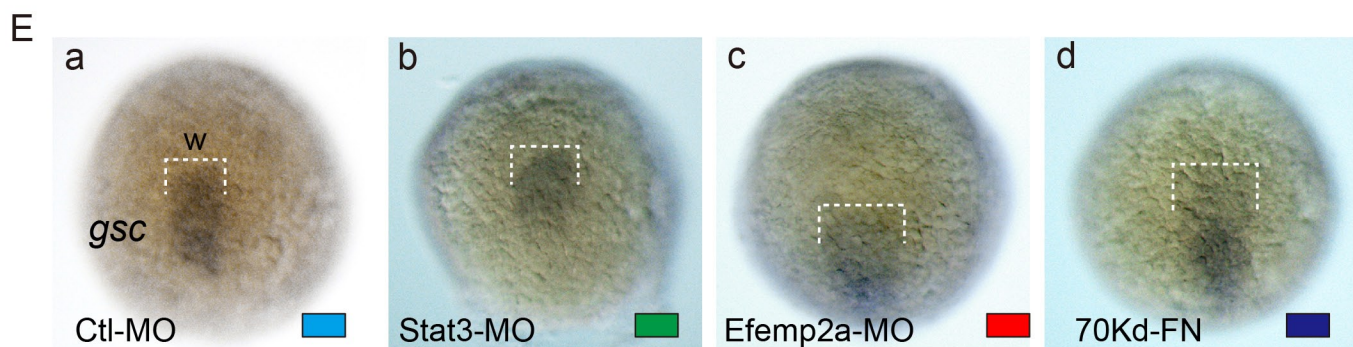
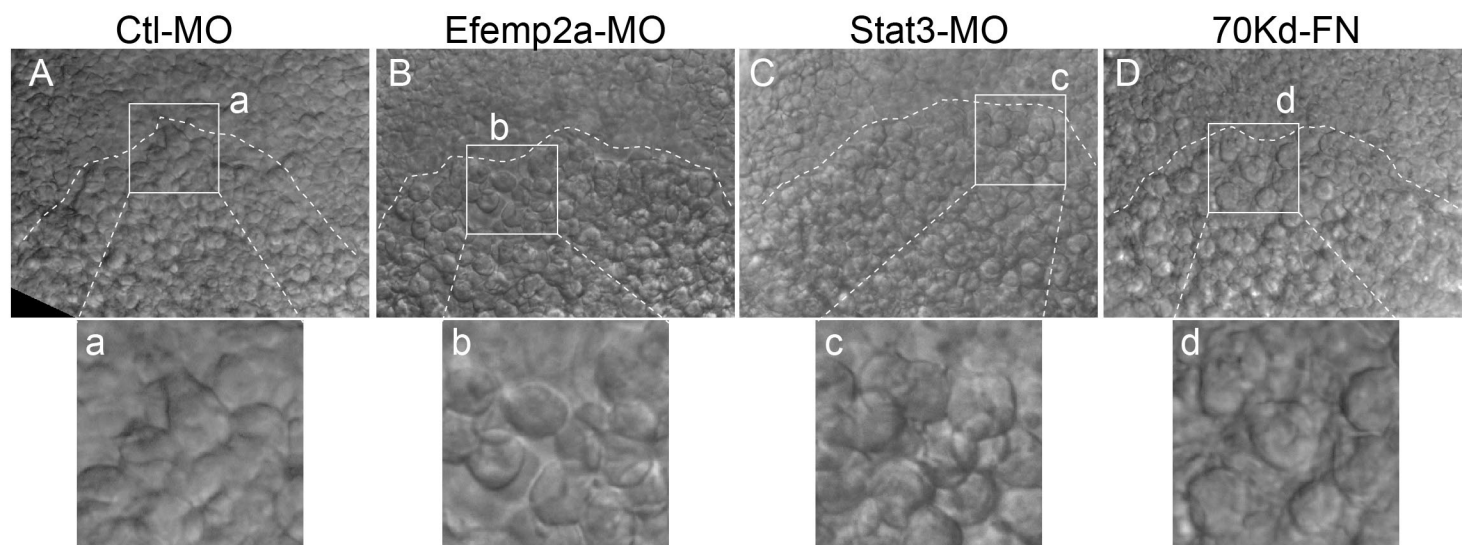
Sfigure 3



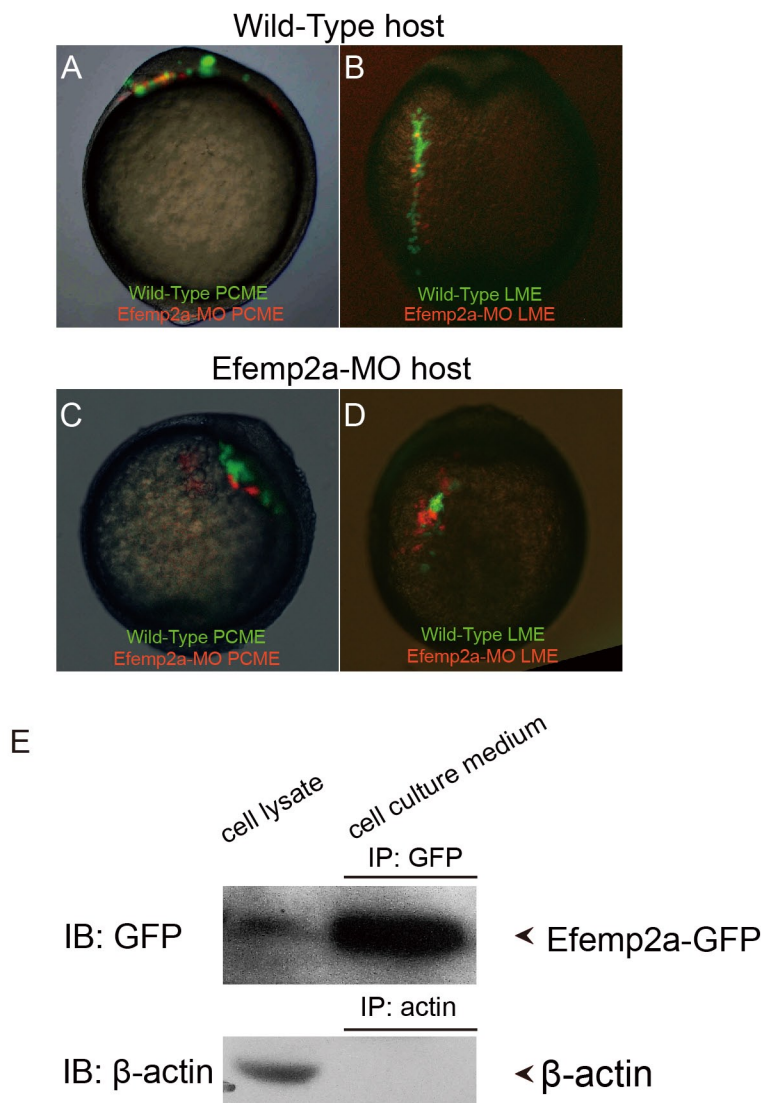
Sfigure 4



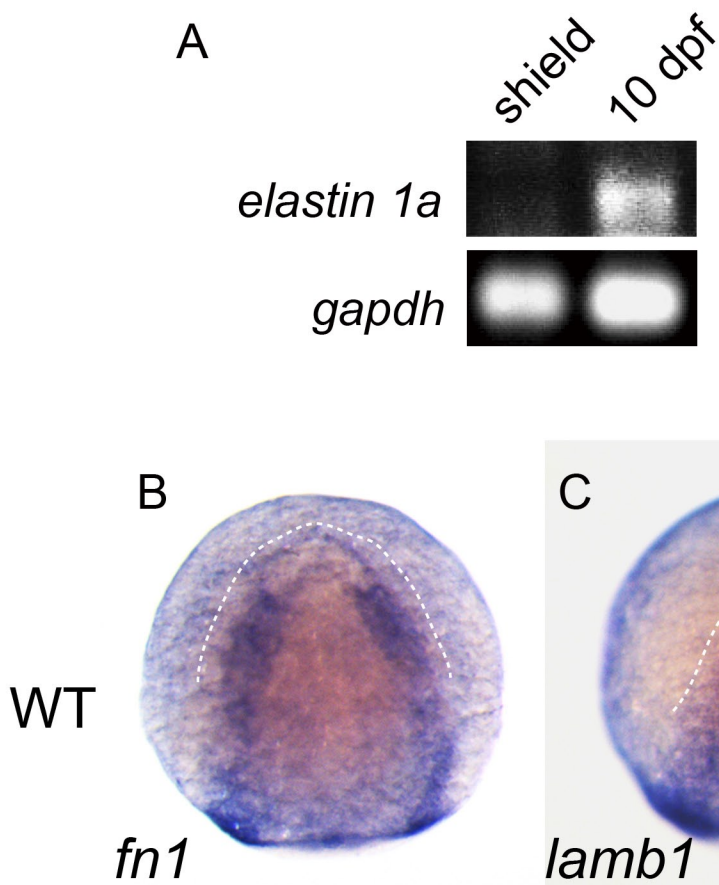
Sfigure 5



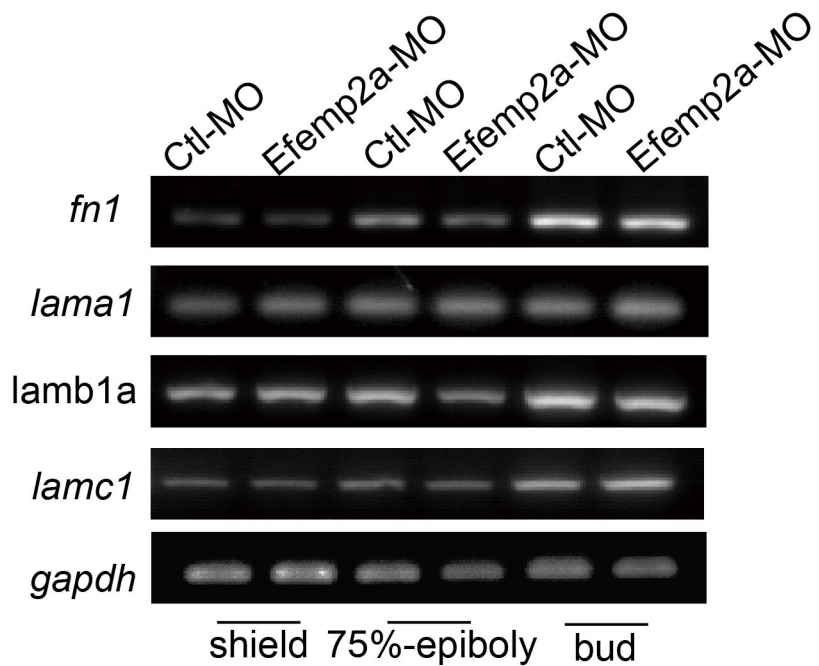
Sfigure 6



Sfigure 7

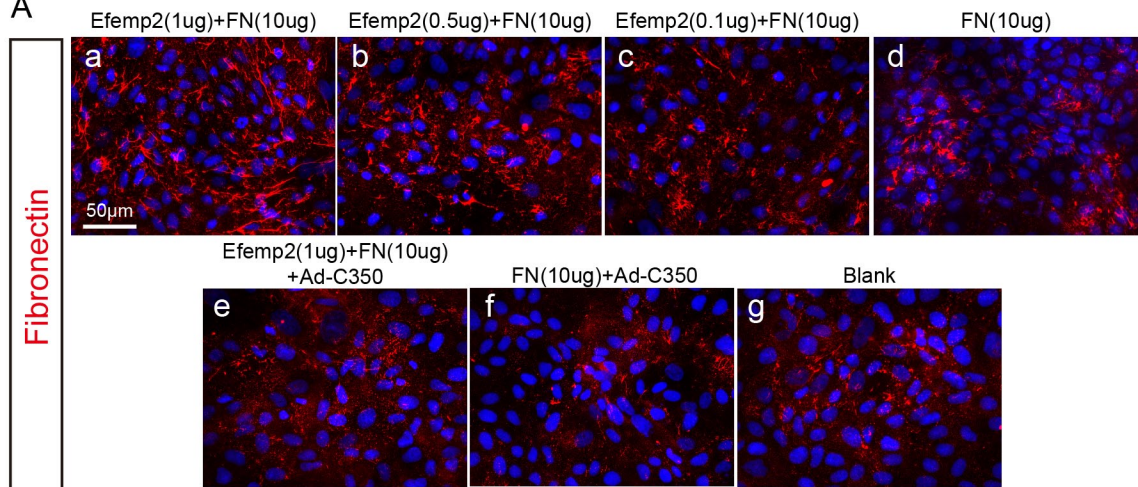


Sfigure 8

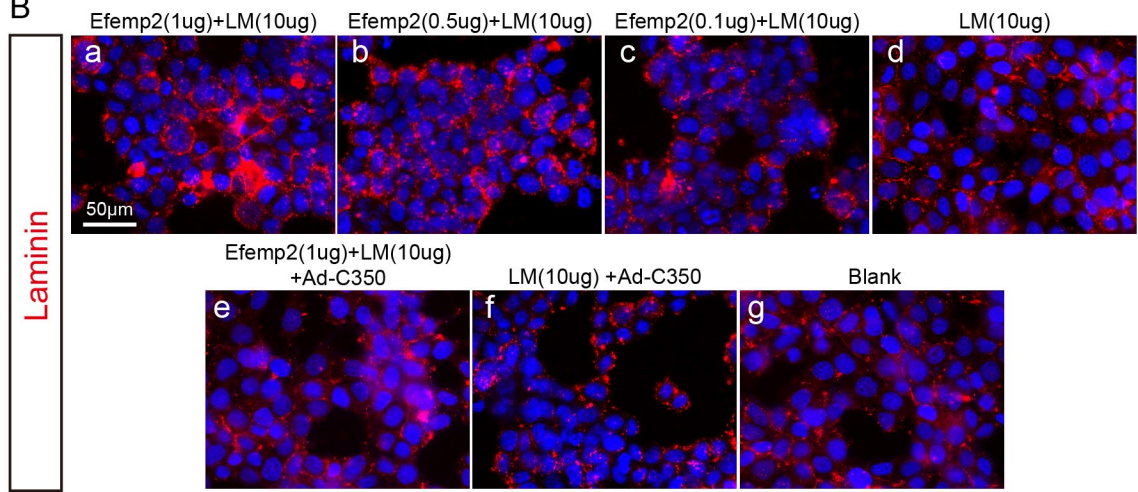


Sfigure 9

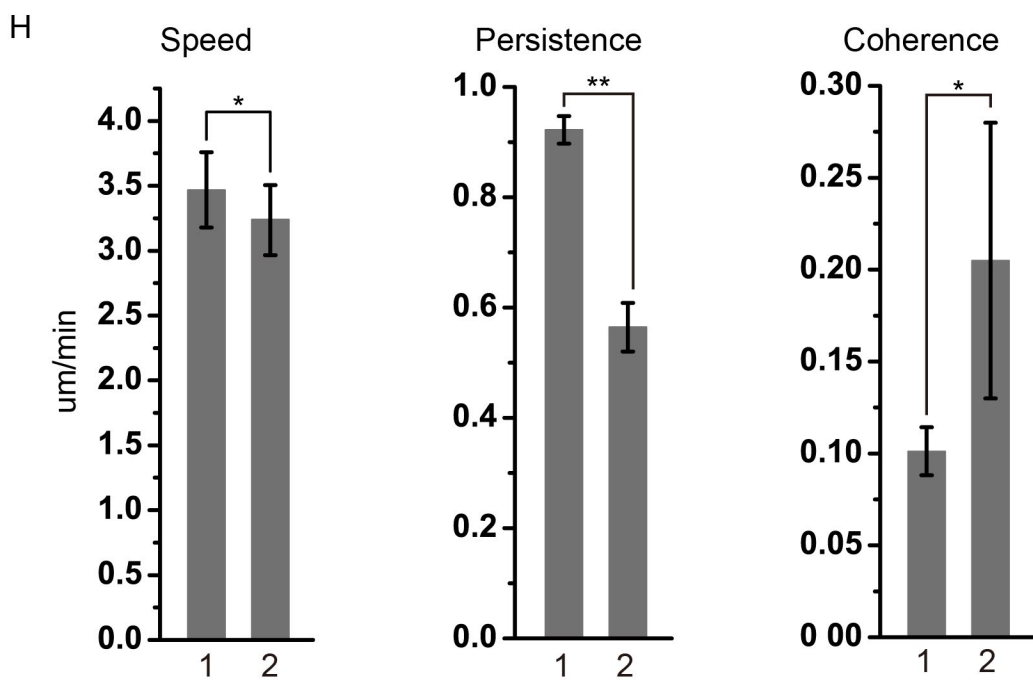
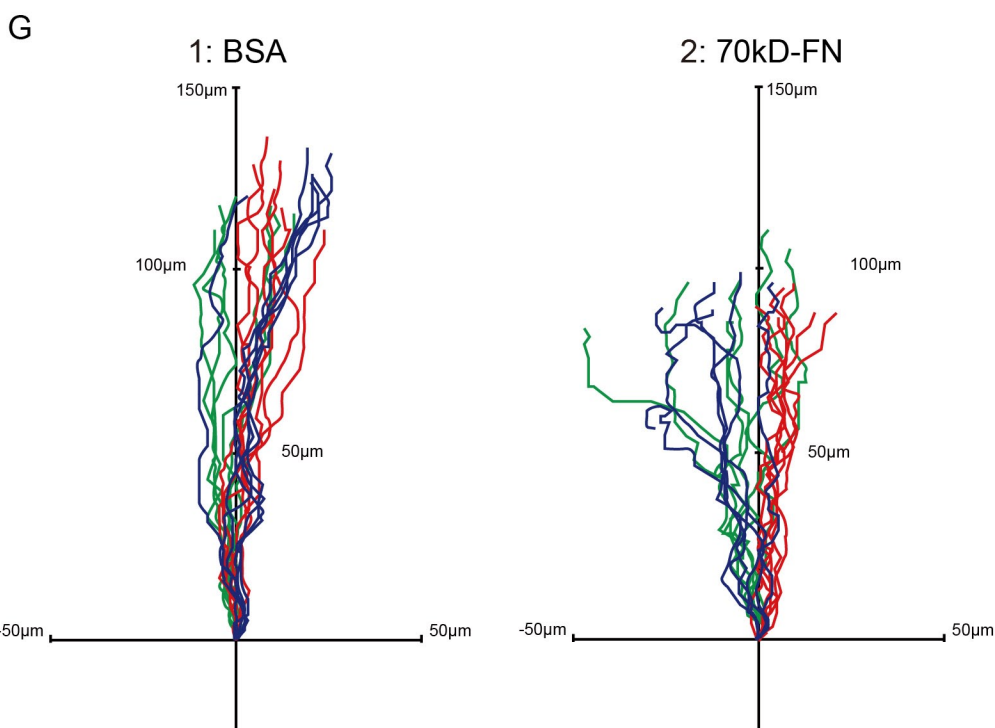
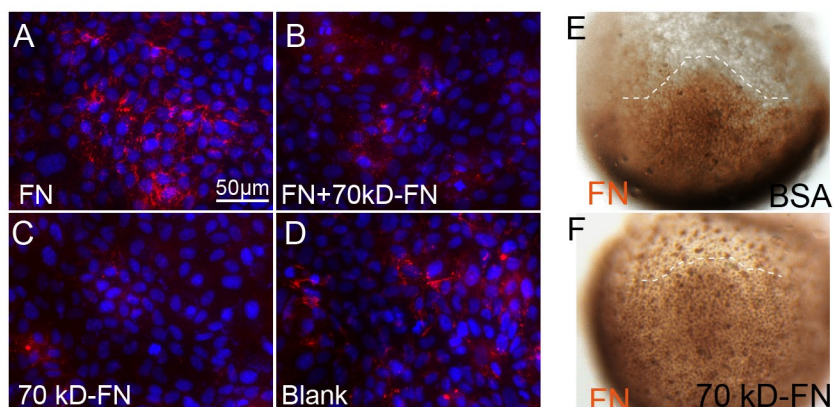
A

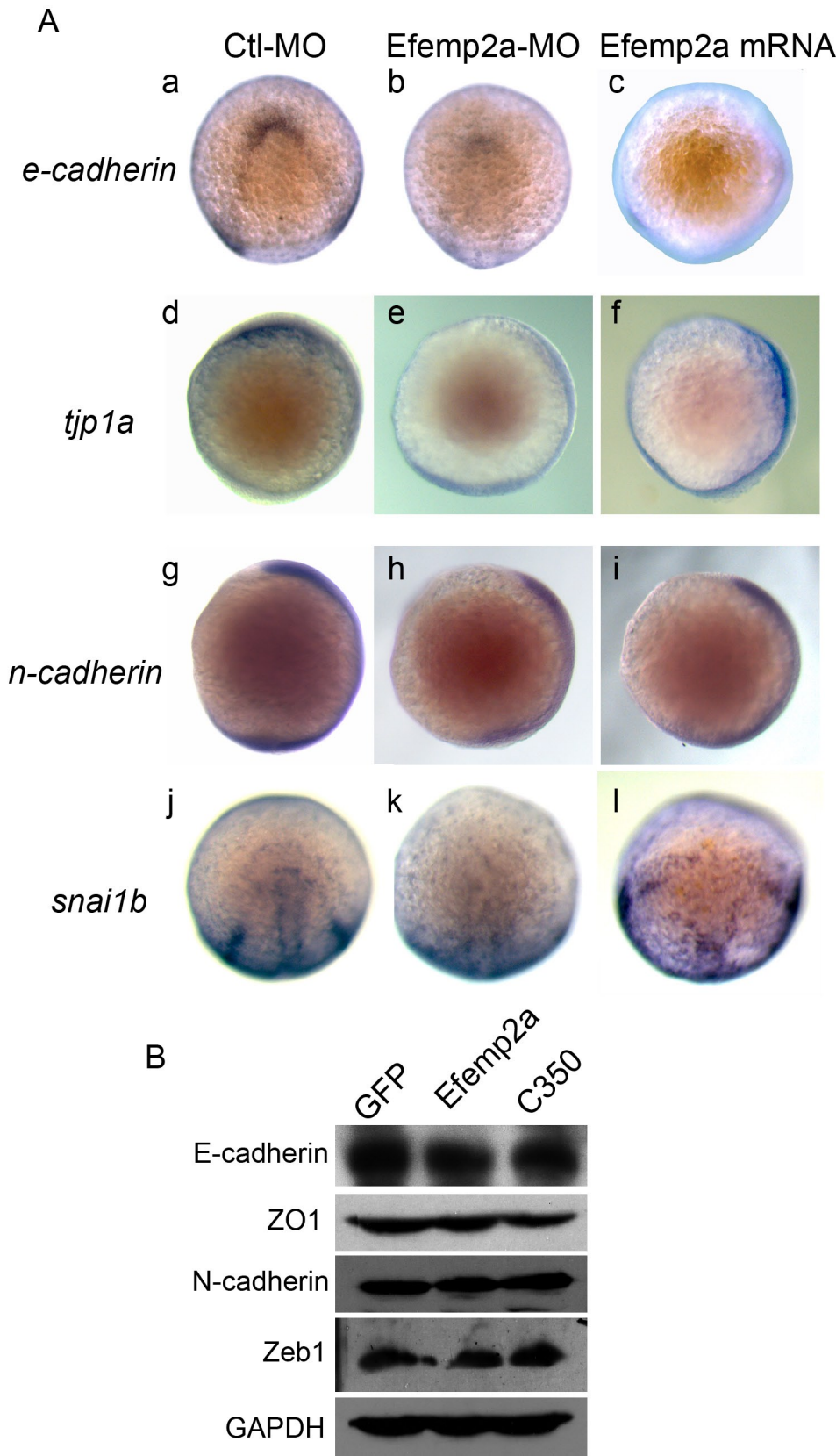


B

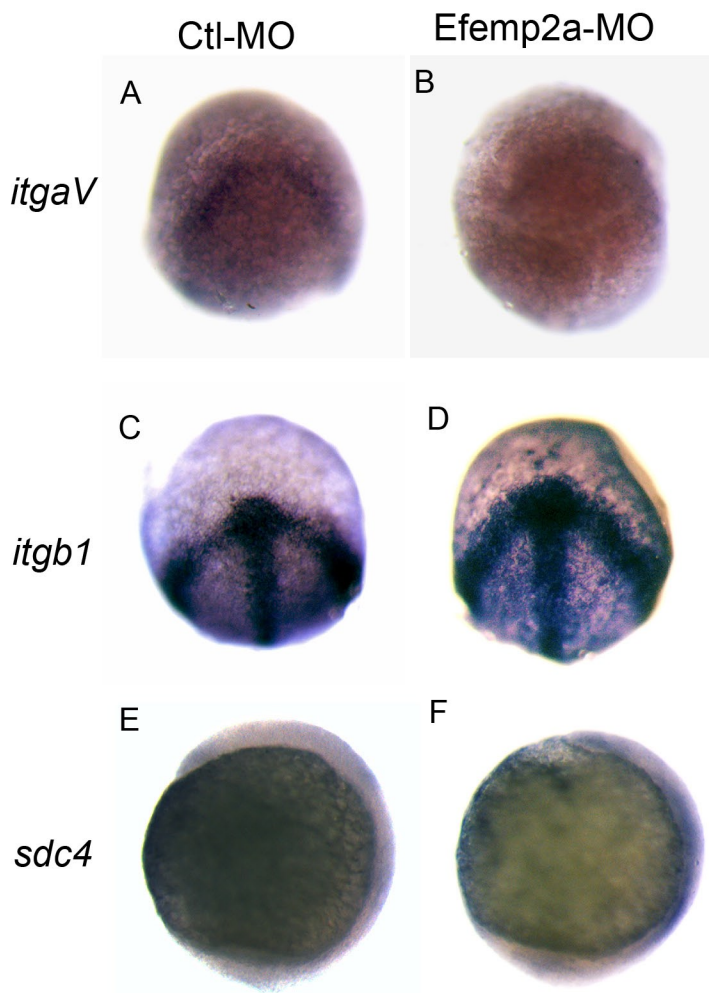


Sfigure 10





Sfigure 12



Sfigure 13

